

# **The 1200 °C Isothermal Sections of the Ni-Al-Cr and the Ni-Al-Mo Ternary Phase Diagrams**

## **THESIS**

Presented in Partial Fulfillment of the Requirements for the Master of Science Degree in  
the Graduate School of The Ohio State University

By

Richard Wendel Cutler

Graduate Program in Materials Science and Engineering

The Ohio State University

2011

Master's Examination Committee:

Professor Ji-Cheng Zhao, Advisor  
Professor Yunzhi Wang

Copyright by  
Richard Wendel Cutler  
2011

# Abstract

The Ni-rich corner of the 1200 °C isothermal sections of both the Ni-Al-Cr and Ni-Al-Mo ternary phase diagrams were obtained using diffusion multiples together with SEM imaging and electro-probe microanalysis (EPMA). In the Ni-Al-Cr system, composition regions of both the Cr-based bcc phase and the  $\beta$ -NiAl phase were observed to be very different from those reported in the literature. For instance, the bcc phase was found to have ~ 26 at% Ni solubility, more than double what has been previously reported in the literature and more consistent with the binary Ni-Cr phase diagram. In the Ni-Al-Mo system a new phase was discovered. This phase,  $\text{Ni}_5\text{Al}_2\text{Mo}_8$ , exists in what appears to be a near stoichiometric composition. Its structure is yet to be determined. Reliable phase equilibrium information useful for superalloy development, especially the phase boundary between the fcc ( $\gamma$ ) phase and the  $L1_2$  ( $\gamma'$ ) phase was obtained for both ternary systems.

For Ralph, Sharon and John Alfred

# Acknowledgements

This document, and my education in its entirety, can be compared to a turtle on a fence post. You may not be entirely sure how I have gotten to this point, but you can be absolutely sure that I did not get here by myself. My acknowledgements begin with my parents. Their love has sustained me. Through everything in school, the hard classes, the late nights, homework, the exams and everything else they have patiently encouraged me to continue working. Each week and occasionally multiple times a week they have called me to check in on me, regardless of what continent they are currently on. They have also set an example for me regarding the importance of education. They did this in two ways, first by attaining degrees themselves and using them, and second by providing me with the opportunity to work in agriculture and learn that I did not want to work manual labor for the rest of my life.

I must also acknowledge my grandfather John Alfred. He passed before I entered Junior High, but he continues to influence and encourage me. He never did attend a university; however, he always encouraged me to attain a degree. One of my most prized possessions is a letter from him, which contains his love for me and his confidence that I will attain a university education. Without this letter and the love it contains I would not have come this far.

I must also thank my sisters and my brother. We have all become busy and we do not always make weekly contact with each other but that has not lessened their support or encouragement.

I would like to thank my Advisor Dr. Ji-Cheng Zhao. He gave me the offer to come to Ohio as a Graduate Research Associate and continue my education at a university that I could not afford on my own. In my two years here he has exercised great patience with me as I learned. Without the guidance and instruction he gave me I would never have understood the material contained in this document or been capable of producing it. He has helped me learn how to do research, to approach questions and intelligently answer them.

I would also like to thank the Air Force and their STW-21 research project for funding my education and my research.

# Vita

May 2002.....Viewmont High School

May 2009.....Bachelor of Science, Materials Science  
and Engineering, University of Utah

May 2009.....Bachelor of Science, Metallurgical  
Engineering, University of Utah

2009 to present.....Graduate Research Associate,  
Department of Materials Science and  
Engineering, The Ohio State University

## Fields of Study

Major Field: Materials Science and Engineering

# Table of Contents

Title Page.....	i
Abstract.....	ii
Dedication.....	iii
Acknowledgements.....	iv
Vita.....	vi
Table of Contents.....	vii
List of Symbols.....	viii
List of Tables.....	ix
List of Figures.....	x
Introduction.....	1
Literature Review.....	4
Experimental Procedures.....	29
Results.....	33
Discussion.....	50
Conclusions.....	54
References.....	57

# List of Symbols

Ni	Atomic symbol for nickel
Al	Atomic symbol for aluminum
Cr	Atomic symbol for chromium
Mo	Atomic symbol for molybdenum
$\gamma$	Terminal nickel phase (fcc)
$\alpha(\text{Cr})$	Terminal chromium phase (bcc)
$\alpha(\text{Mo})$	Terminal molybdenum phase (bcc)
$\gamma'$	Phase in the Ni-Al binary system that has a nominal composition of Ni <sub>3</sub> Al (L1 <sub>2</sub> )
$\beta$	Phase in the Ni-Al binary system that has a nominal composition of NiAl (B2)
$\gamma''$	Phase in the Ni-Mo binary system that has a nominal composition of Ni <sub>3</sub> Mo
$\delta$	Phase in the Ni-Mo binary system that has a nominal composition of NiMo
$\mathcal{K}$	Liquid phase in the phase diagrams by Maslenkov, Udovskii, Burova and Rodimkina
at.%	Atomic percent
wt.%	Weight percent
EPMA	Electro-probe microanalysis
SEM	Scanning electron microscopy

# List of Tables

Table 1	Phase boundary results from the EPMA analysis of the Ni-Al-Cr diffusion multiple. ....	36
Table 2	Three phase equilibrium among the $\gamma$ - $\beta$ - $\alpha$ (Cr) phases. ....	38
Table 3	Three phase equilibrium among the $\gamma$ - $\gamma'$ - $\beta$ phases. ....	38
Table 4	Phase boundary results from EPMA analysis from the Ni-Al-Mo diffusion multiple.....	43
Table 5	Three phase region among the $\gamma$ - $\delta$ - $\alpha$ (Mo) phases. ....	45
Table 6	Three phase region among the $\gamma$ - $\gamma'$ - $\alpha$ (Mo) phases. ....	45
Table 7	Three phase region among the $\beta$ -Ni <sub>5</sub> Al <sub>2</sub> Mo <sub>8</sub> - $\alpha$ (Mo) phases. ....	45
Table 8	Three phase region among the $\gamma'$ -Ni <sub>5</sub> Al <sub>2</sub> Mo <sub>8</sub> - $\alpha$ (Mo) phases. ....	46
Table 9	Three phase region among the $\gamma'$ - $\beta$ -Ni <sub>5</sub> Al <sub>2</sub> Mo <sub>8</sub> phases. ....	46

# List of Figures

Figure 1	The Ni-rich corner of the Ni-Al-Mo phase diagram at 927 °C showing the inconsistency between the phase diagram and the phase compositions obtained by Fährmann <i>et al.</i> ....	2
Figure 2	The Ni-rich corner of the Ni-Al-Cr ternary phase diagram from Wu <i>et al.</i> showing lack of consistency in the phase boundaries. ....	2
Figure 3	The Ni-Al binary phase diagram.....	5
Figure 4	The Ni-Cr binary phase diagram.....	6
Figure 5	The Al-Cr binary phase diagram.....	7
Figure 6	The Ni-Mo binary phase diagram.....	8
Figure 7	The Al-Mo binary phase diagram.....	8
Figure 8	The Ni-Al-Cr ternary phase diagram at 1423 K by Oforika and Argent....	10
Figure 9	The Ni-Al-Cr ternary phase diagram at 1423 K by Oforika and Haworth.	10
Figure 10	The Ni-rich corner of the Ni-Al-Cr ternary phase diagram at 1400 K by Hong <i>et al.</i> .....	11
Figure 11	The Ni-rich corner of the Ni-Al-Cr ternary phase diagram at 1300 K by Hong <i>et al.</i> .....	11
Figure 12	The $\gamma$ solvus lines for the Ni-Al-Cr ternary system by Hong <i>et al.</i> ....	12
Figure 13	Phase boundaries in the Ni-rich corner of the Ni-Al-Cr ternary system at 1100 and 1300 °C by Jia, Ishida and Nishizawa (Note that these diagrams are plotted in wt.% instead of at.%). ....	13
Figure 14	The Ni-rich corner of the Ni-Al-Cr ternary phase diagram at 900 °C by Brož <i>et al.</i> .....	14

Figure 15	The Ni-Al-Cr ternary phase diagram at 1150 °C by Grushko <i>et al.</i> .....	15
Figure 16	The Ni-Al-Mo ternary phase diagram at 1473 K by Nash <i>et al.</i> .....	16
Figure 17	The Ni-Al-Mo ternary phase diagram at 1260 °C by Miracle <i>et al.</i> .....	17
Figure 18	The Ni-Al-Mo ternary phase diagram at 1171 °C by Miracle <i>et al.</i> .....	17
Figure 19	The Ni-Al-Mo ternary phase diagram at 1093 °C by Miracle <i>et al.</i> .....	18
Figure 20	The Ni-Al-Mo ternary phase diagram at 1036 °C by Miracle <i>et al.</i> .....	18
Figure 21	The Ni-Al-Mo ternary phase diagram at 927 °C by Miracle <i>et al.</i> .....	18
Figure 22	The Ni-Al-Mo ternary phase diagram at 1300 °C by Maslenkov and Rodimkina.....	20
Figure 23	The Ni-Al-Mo ternary phase diagram at 1390 °C by Maslenkov, <i>et al.</i> .....	21
Figure 24	The Ni-Al-Mo ternary phase diagram at 1380 °C by Maslenkov <i>et al.</i> .....	21
Figure 25	The Ni-Al-Mo ternary phase diagram at 1360 °C by Maslenkov <i>et al.</i> .....	22
Figure 26	The Ni-Al-Mo ternary phase diagram at 1340 °C by Maslenkov <i>et al.</i> .....	23
Figure 27	The Ni-Al-Mo ternary phase diagram at 1200 °C by Maslenkov <i>et al.</i> .....	24
Figure 28	The Ni-Al-Mo ternary phase diagram at 1100 °C by Maslenkov <i>et al.</i> .....	24
Figure 29	The Ni-Al-Mo ternary phase diagram at 880 °C by Maslenkov <i>et al.</i> .....	25
Figure 30	The Ni-Al-Mo ternary phase diagram at 700 °C by Maslenkov <i>et al.</i> .....	26
Figure 31	The Ni-rich corner of the Ni-Al-Mo ternary phase diagram at 1400 K by Hong <i>et al.</i> .....	27
Figure 32	The Ni-rich corner of the Ni-Al-Mo ternary phase diagram at 1300 K by Hong <i>et al.</i> .....	28
Figure 33	Solvus lines for the $\gamma'$ phase in the Ni-Al-Mo ternary system by Hong <i>et al.</i> .....	28
Figure 34	SEM image of the Ni-Al-Cr diffusion multiple used to identify positions for EPMA line scans.....	30
Figure 35	SEM image of the Ni-Al-Mo diffusion multiple used to identify positions for EPMA line scans.....	31
Figure 36	EPMA results for line scan 15 on the Ni-Al-Cr diffusion multiple at 1200 °C showing composition vs. relative distance of the scan.....	34

Figure 37	EPMA results for line scan 15 on the Ni-Al-Cr diffusion multiple at 1200 °C in a triangular composition vs. composition plot (Data are plotted in at.% axes. The lower left corner is Ni, Lower right is Al, and top is Cr).....	35
Figure 38	Tie lines for the Ni-Al-Cr ternary phase diagram at 1200 °C.....	38
Figure 39	The Ni-Al-Cr ternary phase diagram at 1200 °C.....	39
Figure 40	The Ni-rich corner of the Ni-Al-Cr ternary phase diagram at 1200 °C.....	40
Figure 41	EPMA results for line scan # 10 on the Ni-Al-Mo diffusion multiple at 1200 °C showing composition vs. relative distance of the line scan.....	41
Figure 42	EPMA results for line scan # 10 on the Ni-Al-Mo diffusion multiple at 1200 C in a triangular composition vs. composition plot (Data are plotted in at.% axes. The lower left corner is Ni, lower right is Al, and top is Mo).....	42
Figure 43	Tie lines for the Ni-Al-Mo ternary phase diagram at 1200 °C.....	44
Figure 44	The Ni-Al-Mo ternary phase diagram at 1200 °C.....	48
Figure 45	The Ni-rich corner of the Ni-Al-Mo ternary phase diagram at 1200 °C.....	49
Figure 42	Calculated 1200 °C isothermal section of the Ni-Al-Cr ternary system based on the thermodynamic assessment of Huang and Chang.....	56

# Introduction

Phase diagrams are a powerful tool for designing alloys for both structural and multifunctional applications. They provide equilibrium phase stability regions as well as the multi-phase regions for a given system. Phase diagrams can be easily plotted for binary and ternary systems. For higher order systems, multi-dimensional plots are no longer convenient for two dimensional or space. This challenge can be circumvented by pseudo-binary or pseudo-ternary phase diagrams. More recently, modeling software such as Thermo-Calc® has been used to determine phase stability in multicomponent alloys. The major challenge associated with this approach is that the calculated phase stability is only as reliable as the database that is being used. Hence, if the database is unreliable then none of the calculations can be trusted. Thus there is a great need for reliable thermodynamic data, especially reliable phase stability data.

Aluminum, chromium and molybdenum are among the most important alloying elements for Ni-base superalloys for jet engine and land-based gas turbine applications, thus reliable Ni-Al-Cr and Ni-Al-Mo ternary phase diagrams are important for reliable design of superalloys. In 1997 Fährmann *et al*<sup>1</sup> published a paper on precipitation in Ni-Al-Mo alloys. One of their observations was that the  $\gamma/\gamma+\gamma'$  phase boundary was inconsistent with their experimental results, indicating that the phase boundary data in the literature were not reliable, as shown in Figure 1. This problem has not been addressed yet in the literature.

Similar lack of consensus was pointed out by Wu *et al.*<sup>2</sup> for the Ni-rich corner of the Ni-Al-Cr system as shown in Figure 2.

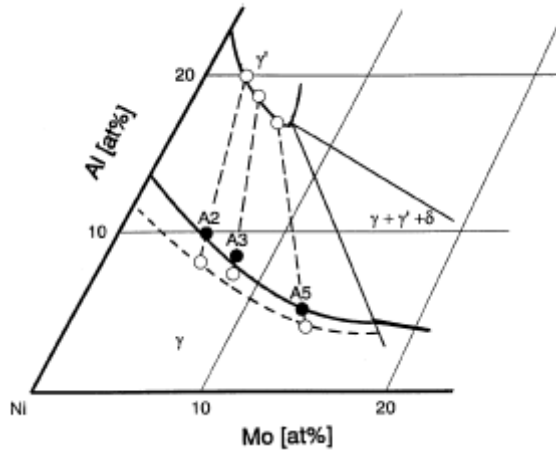


Figure 1 The Ni-rich corner of the Ni-Al-Mo phase diagram at 927 °C showing the inconsistency between the phase diagram and the phase compositions obtained by Fährmann *et al.*

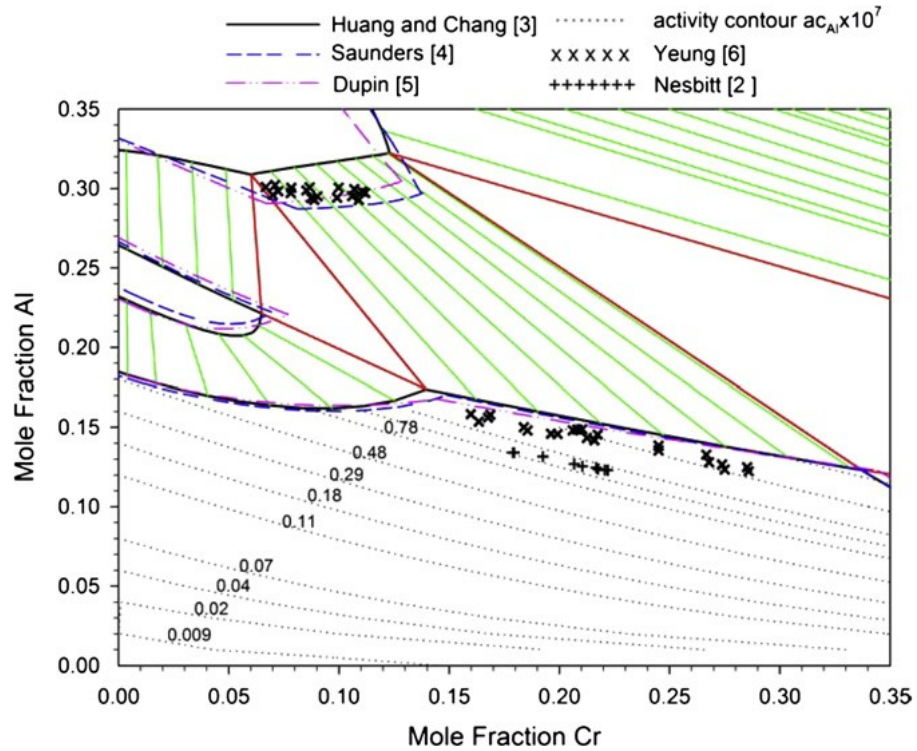


Figure 2 The Ni-rich corner of the Ni-Al-Cr ternary phase diagram from Wu *et al.* showing lack of consistency in the phase boundaries.

The present work was undertaken to obtain reliable phase diagram data at the Ni-rich corner of both the Ni-Al-Cr and Ni-Al-Mo systems. The samples used in this study were prepared by long-term annealing treatments to examine the phase boundaries at equilibrium in the ternary systems. Results obtained from such long-term annealed samples are supposed to provide more reliable phase equilibrium data.

# Literature Review

## **Binary Systems:**

The binary Ni-Al, Ni-Cr, Al-Cr, Ni-Mo, and Al-Mo systems pertinent to both Ni-Al-Cr and Ni-Al-Mo ternary systems are briefly discussed here. These systems set the boundary conditions for the ternary systems. The Ni-Al binary system is the base for Ni-based superalloys. The  $\gamma'$  ( $\text{Ni}_3\text{Al}$ ) precipitation from the  $\gamma$  (fcc) matrix provides the major strengthening mechanism for Ni-based superalloys. The Ni-Al phase diagram is shown in Fig. 3 which is the result of a significant number of studies. The important features in Figure 3 that are pertinent to this study are the solubility limits for the  $\gamma$ ,  $\gamma'$ , and  $\beta$  phases.

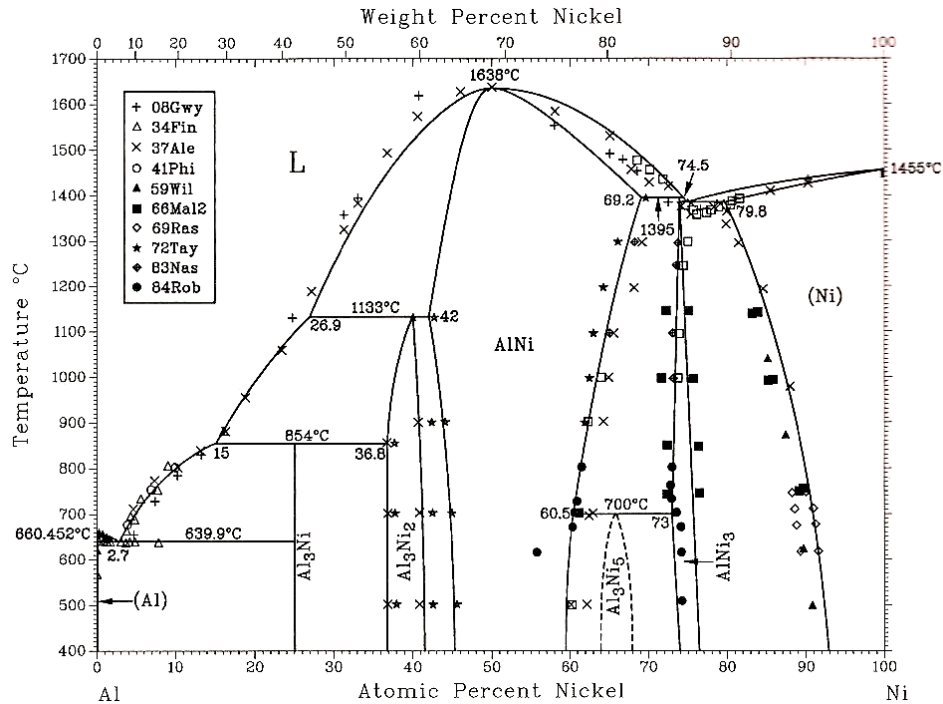


Figure 3. The Ni-Al binary phase diagram.<sup>3</sup>

The Ni-Cr binary phase diagram is shown in Figure 4 with several sets of experimental data superimposed. This diagram shows a dramatic temperature dependency of the solubility of Ni in the  $\alpha$ (Cr) phase in the temperature range between 1100 and 1300 °C. There is less dramatic, but still significant change of Cr solubility in the  $\gamma$  phase. At 1200 °C, which is the temperature of the current study, the Ni solubility in bcc (Cr) and the Cr solubility in fcc (Ni) is ~ 26 at.% and ~48 at.%, respectively. Those data will be important to check the reliability of the ternary phase diagram data.

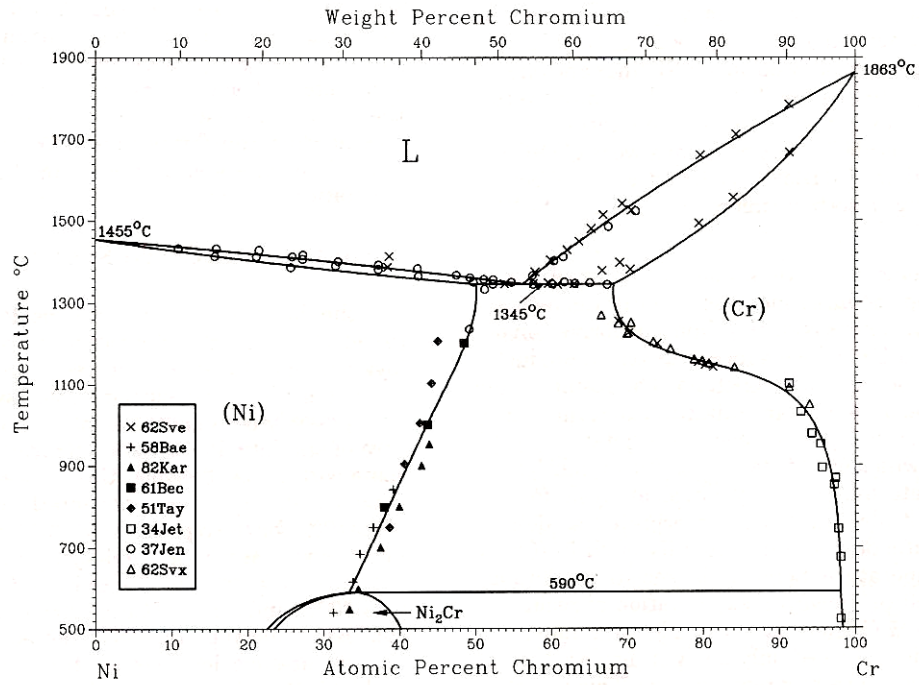


Figure 4. The Ni-Cr binary phase diagram.<sup>3</sup>

The Al-Cr binary system is shown in Figure 5. The important feature in this phase diagram pertinent to this study is the Al solubility in the  $\alpha$ (Cr) phase which is about 43 at.% at 1200 °C.

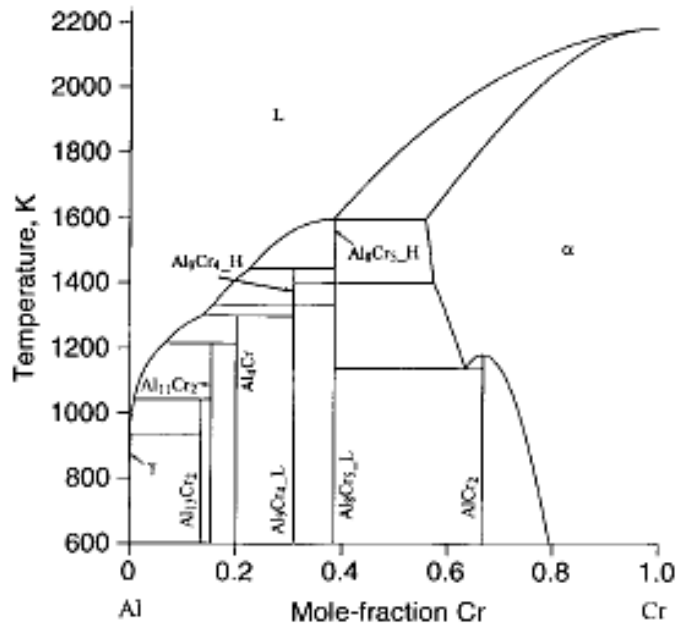


Figure 5. The Al-Cr binary phase diagram.<sup>4</sup>

For the Ni-Al-Mo system, the Ni-Al binary is repeated. The Ni-Mo phase diagram is shown in Figure 6. The solubility limits of the  $\gamma$ ,  $\delta$ , and  $\alpha(\text{Mo})$  phases are important to the present study. There is only limited solubility Ni in Mo (e.g., 2 at.% at 1200 °C), but the solubility of Mo in g (Ni) is quite high, ~26 at.% at 1200 °C. The  $\delta$ -MoNi intermetallic phase has a limited, but relatively poorly defined composition range from ~52 to 54 at.% Mo.

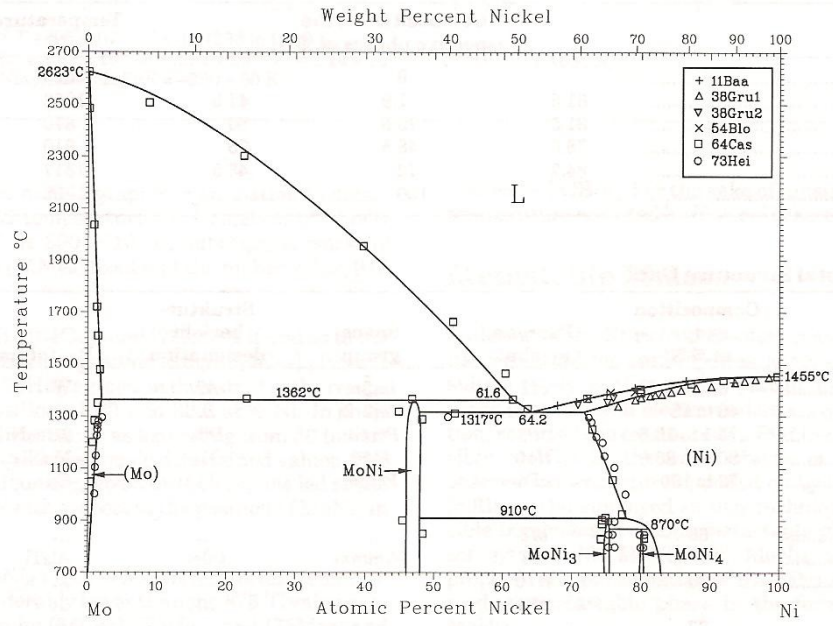


Figure 6. The Ni-Mo phase diagram.<sup>3</sup>

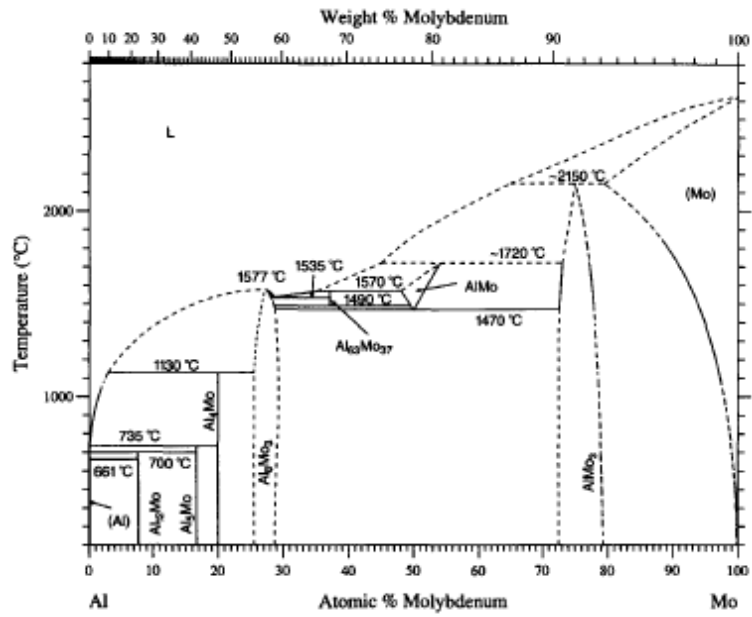


Figure 7. The Al-Mo phase diagram.<sup>5</sup>

Figure 7 is the Al-Mo binary diagram which shows a strong temperature dependency of the Al solubility in  $\alpha(\text{Mo})$ . At 1200 °C, the solubility is  $\sim 3$  at.%. The composition range of the  $\text{Mo}_3\text{Al}$  phase is still ill-defined.

### **The Ni-Al-Cr Ternary System:**

Oforika and Argent<sup>6</sup> determined the Ni-Al-Cr ternary phase diagram at 1200 °C (1473 K), as shown in Figure 8. They show that there are no ternary phases present in this ternary system. There is a large two phase region between the  $\beta$  and  $\alpha(\text{Cr})$  phases. The Ni solubility limit in the  $\alpha(\text{Cr})$  phase in Figure 8 is only  $\sim 13$  at.% which is far from  $\sim 26$  at.% that is expected from the binary Ni-Cr phase diagram (Figure 4).

Two years after Figure 8 was published, Oforika and Haworth<sup>7</sup> published a follow up phase diagram at 1423 K, Figure 9. This diagram shows similar discrepancy in the Ni solubility limit in the  $\alpha(\text{Cr})$  phase. The overall phase diagram features are the same as those in Figure 8.

These investigations were supplemented by the work of Hong, Mishima and Suzuki<sup>8</sup> in the Ni-rich corner. The work of Hong *et al.* was undertaken to determine the two-phase regions between the  $\gamma$  and  $\gamma'$  phases, and the  $\gamma'$  and  $\beta$  phases. They also determined the  $\gamma'$  solvus lines with regard to the  $\gamma$  matrix.

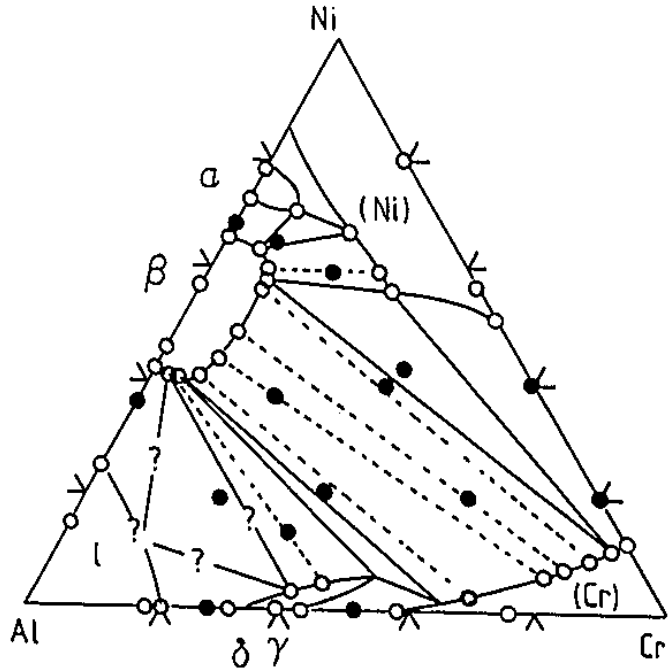


Figure 8. The Ni-Al-Cr ternary phase diagram at 1423 K by Oforka and Argent.

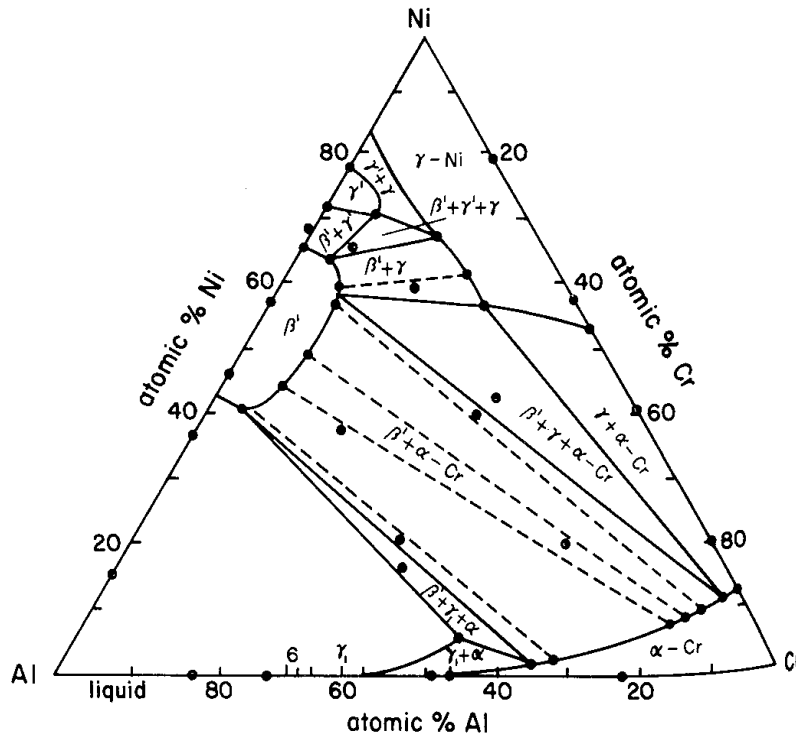


Figure 9. The Ni-Al-Cr ternary phase diagram at 1423 K by Oforka and Haworth.

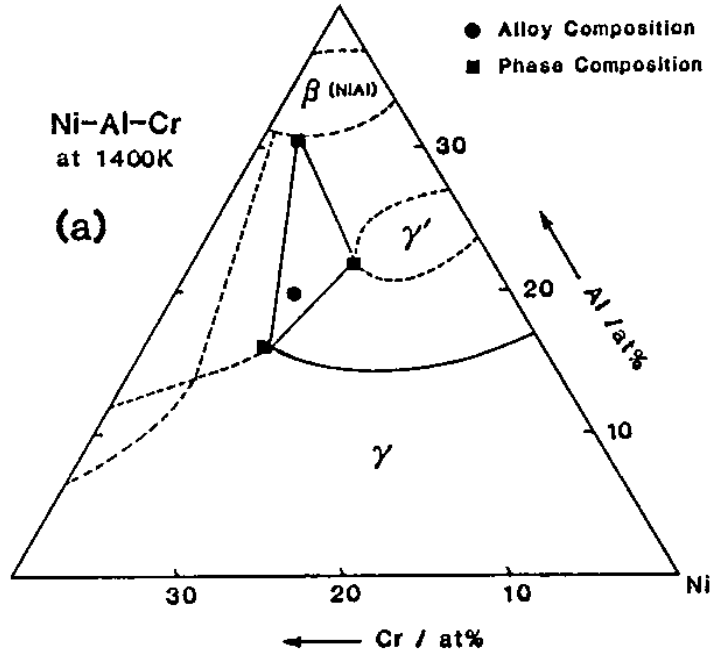


Figure 10 Ni-rich corner of the Ni-Al-Cr ternary phase diagram at 1400 K by Hong *et al.*

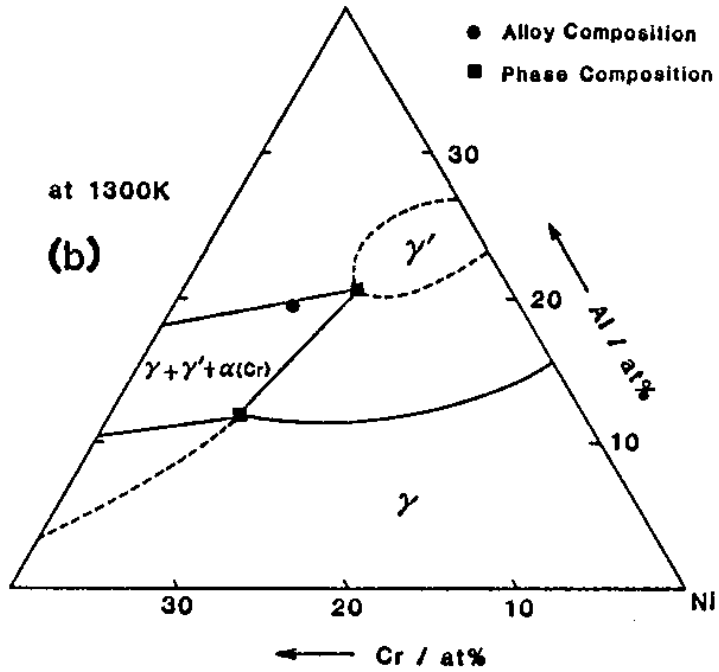


Figure 11 Ni-rich corner of the Ni-Al-Cr ternary phase diagram at 1300 K by Hong *et al.*

A comparison of Figures 10 and 11 shows that there is a change in phase stability between 1300 and 1400 K. At 1400 K the three-phase region is between the  $\gamma$ ,  $\gamma'$ , and  $\beta$  phases, while at 1300 K the three-phase region is between the  $\gamma$ ,  $\gamma'$ , and  $\alpha(\text{Cr})$  phases. The Cr solubility in the  $\gamma'$  phase does not change much between the two temperatures. However, it should be mentioned that these studies are based on a single alloy at each temperature in the three-phase region.

Figure 12 from Hong *et al.* shows the progression of iso-solvus lines (solvus projection) of the  $\gamma/\gamma-\gamma'$  phase boundary. It clearly shows the increase Al solubility in the  $\gamma$  phase with increasing temperature.

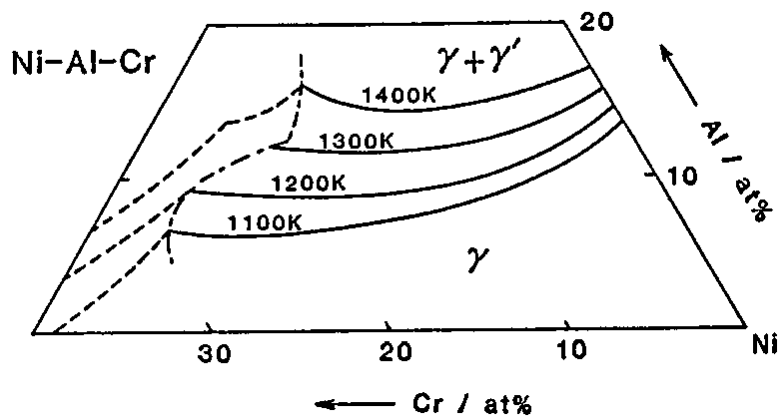


Figure 12. The  $\gamma$  solvus lines for the Ni-Al-Cr ternary system by Hong *et al.*

Jia, Ishida and Nishizawa determined the phase boundaries of the  $\gamma$ - $\gamma'$  and  $\gamma'$ - $\beta$  two phase regions at 1300 and 1100 °C. Their phase diagrams are plotted in wt.% axes instead of at.% axes as most other phase diagrams.

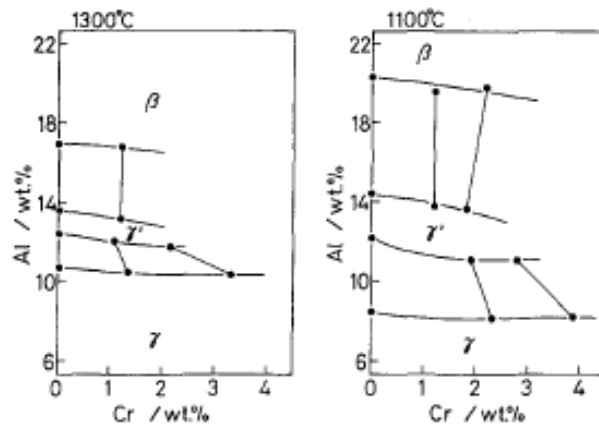


Figure 13. Phase boundaries in the Ni-rich corner of the Ni-Al-Cr ternary system at 1100 and 1300 °C by Jia, Ishida and Nishizawa (Note that these diagrams are plotted in wt.% instead of at.%).

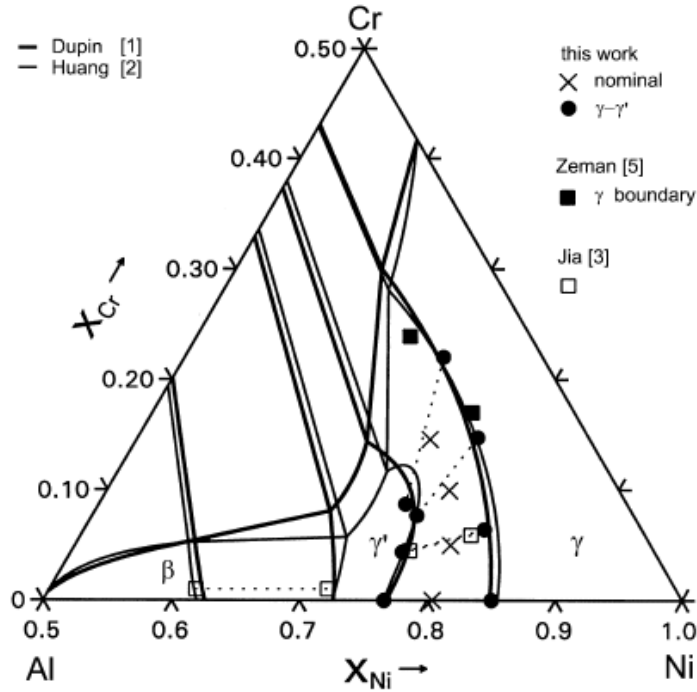


Figure 14. The Ni-rich corner of the Ni-Al-Cr ternary phase diagram at 900 °C by Brož *et al.*

Brož *et al.*<sup>9</sup> compared their own experimental results with four other studies in the literature in Figure 14. Their study was performed at 900 °C, a temperature much lower than the current work (1200 °C); but their work shows that the phase boundaries do not agree with each other, especially for the calculated phase diagrams of Dupin vs Huang. This further illustrates the need for accurate determination of the phase boundaries of the Ni-Al-Cr system.

Grushko *et al.*<sup>10</sup> made a comparison of 1150 °C isothermal sections of the Ni-Al-Cr ternary system from various source as shown in Figure 15. They showed higher

solubility of Ni in the  $\alpha(\text{Cr})$  phase than that reported previously, but still much lower than what's expected from the binary phase diagram (Figure 4). They also show significant disagreement in the shape of the other phases present, which calls for further investigation of this system.

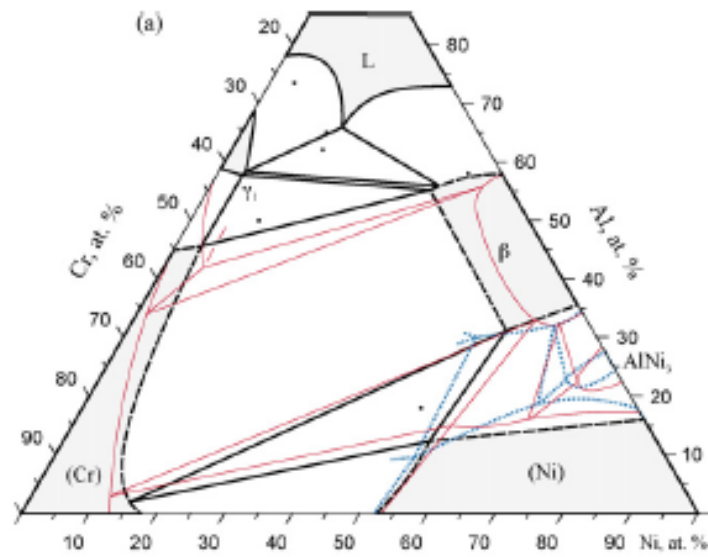


Figure 15. The Ni-Al-Cr ternary phase diagram at 1150 °C by Grushko *et al.*

## The Ni-Al-Mo Ternary System:

The Ni-Al-Mo system was studied by Nash, Fielding and West<sup>11</sup> in 1983. They reported the Ni-rich corner of an isothermal section at 1200 °C, Figure 16. The phases present are  $\gamma$ ,  $\gamma'$ ,  $\beta$ ,  $\delta$ , and  $\alpha(\text{Mo})$ . The  $\text{AlMo}_3$  phase that is present in the Al-Mo binary diagram is not present in this diagram. The Mo solubility in the  $\beta$  phase is much less than the Cr solubility in the same phase.

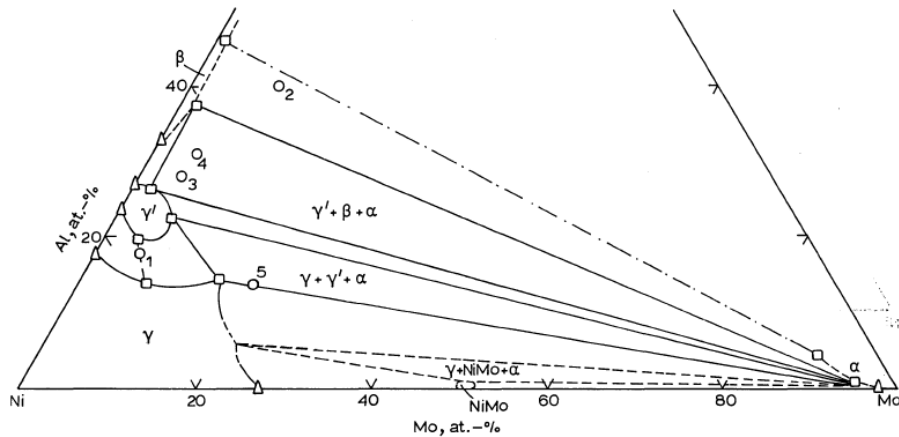


Figure 16. The 1200 °C isothermal section of the Ni-Al-Mo ternary phase diagram by Nash *et al.*

Miracle *et al.*<sup>12</sup> measured the Ni-rich corner of the Ni-Al-Mo ternary system at five different temperatures as shown in Figures 17 to 21. The shapes of the  $\gamma$  and  $\gamma'$

phases in their phase diagrams are significantly different from those reported by Nash *et al.* For instance, the  $\gamma+\gamma'$  two phase region is narrower in Figure 17 than in Figure 16, while the solubility limit of Al in the  $\gamma$  phase is approximately the same. The three-phase regions in the two diagrams are similar and have the same compositions in the diagrams.

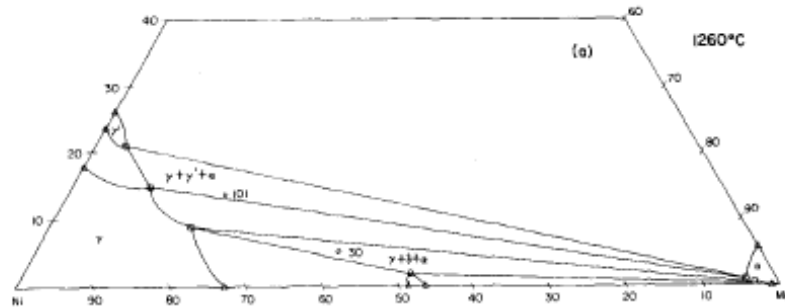


Figure 17. The Ni-Al-Mo ternary phase diagram at 1260 °C by Miracle *et al.*

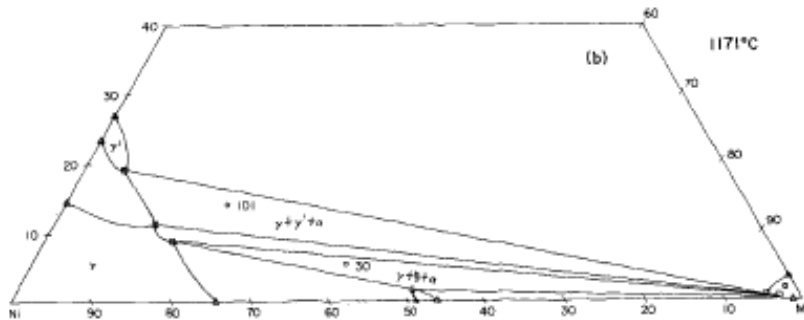


Figure 18. The Ni-Al-Mo ternary phase diagram at 1171 °C by Miracle *et al.*

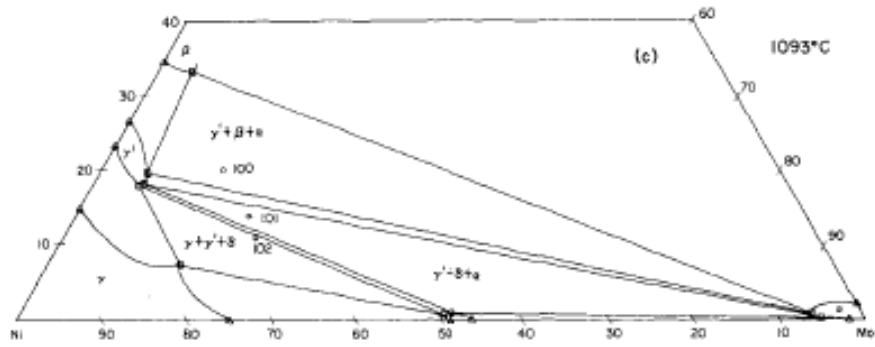


Figure 19. The Ni-Al-Mo ternary phase diagram at 1093 °C by Miracle *et al.*

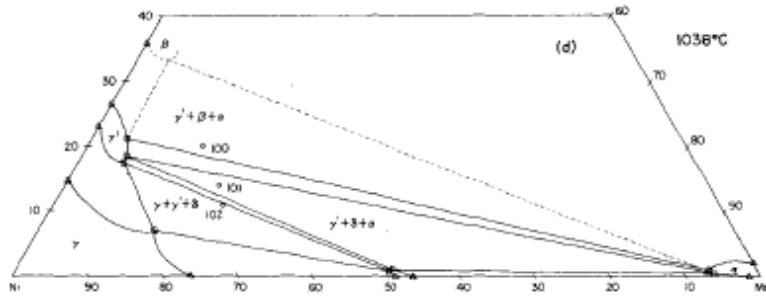


Figure 20. The Ni-Al-Mo ternary phase diagram at 1036 °C by Miracle *et al.*

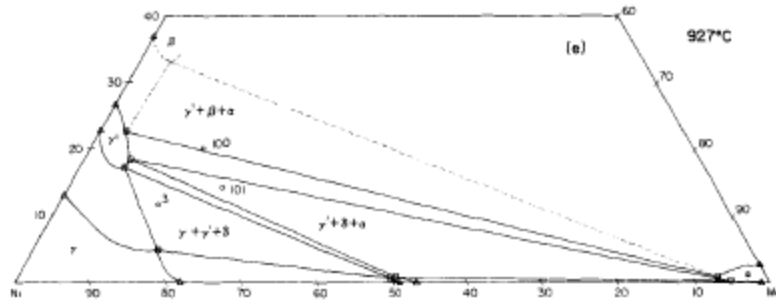


Figure 21. The Ni-Al-Mo ternary phase diagram at 927 °C by Miracle *et al.*

Figures 18 to 21 show unsurprising trends of decreasing solubility of Al and Mo in  $\gamma$ ,  $\delta$ , and  $\alpha(\text{Mo})$  phases as the temperature decreases. The Mo solubility in the  $\gamma'$  phase remains essentially constant except at 1260 °C. Between 1171 and 1093 °C there is a transition in the three-phase regions, from a  $\gamma$ - $\delta$ - $\alpha(\text{Mo})$  three-phase region to a  $\gamma'$ - $\delta$ - $\alpha(\text{Mo})$  three phase region. The phase diagram shown in Figure 21 is the same phase diagram shown in Figure 1. Because of this, the Ni-Al-Mo phase diagram needs further investigation.

Maslenkov and Rodimkina<sup>13</sup> determined the Ni-Al-Mo phase diagram at 1300 °C as shown in Figure 22. The overall topology of this isothermal section agree with that of the previous investigations by Nash *et al.* and Miracle *et al.*, but the shapes of the phase regions and the compositions of the three-phase regions are quite different. This phase diagram should be regarded only as a schematic since there are not enough data points to define the phase boundaries with a high degree of confidence.

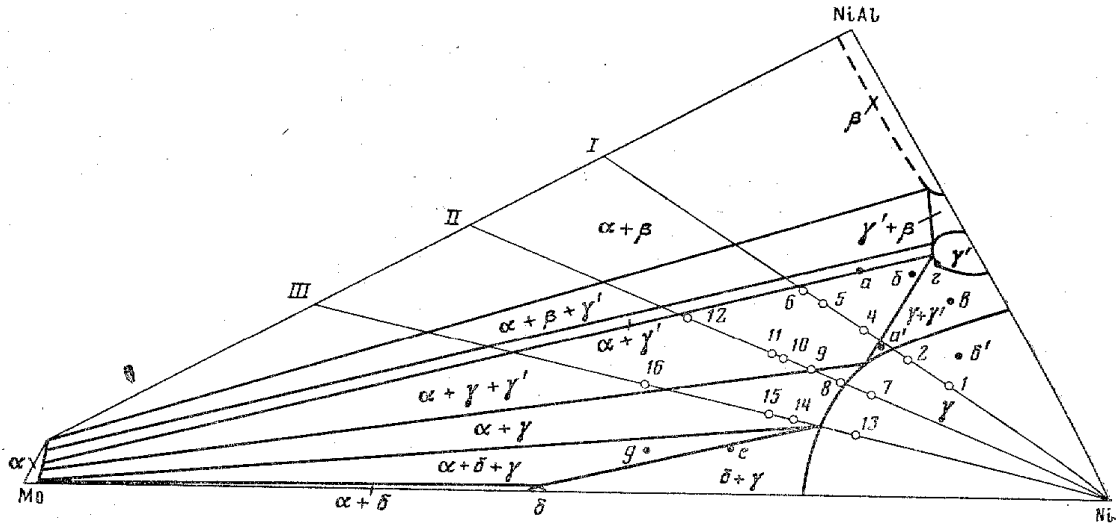


Figure 22. The Ni-Al-Mo ternary phase diagram at 1300 °C by Maslenkov and Rodimkina.

In the same year, Maslenkov and Rodimkina worked with Udovskii and Burova<sup>14</sup> to follow up on this system with four more isothermal sections at 1390, 1380, 1360 and 1340 °C, Figures 23 to 26. These phase diagrams show the appearance of liquid above 1300 °C in the Al-poor region of the diagram. They track the continued melting as the temperature increases.



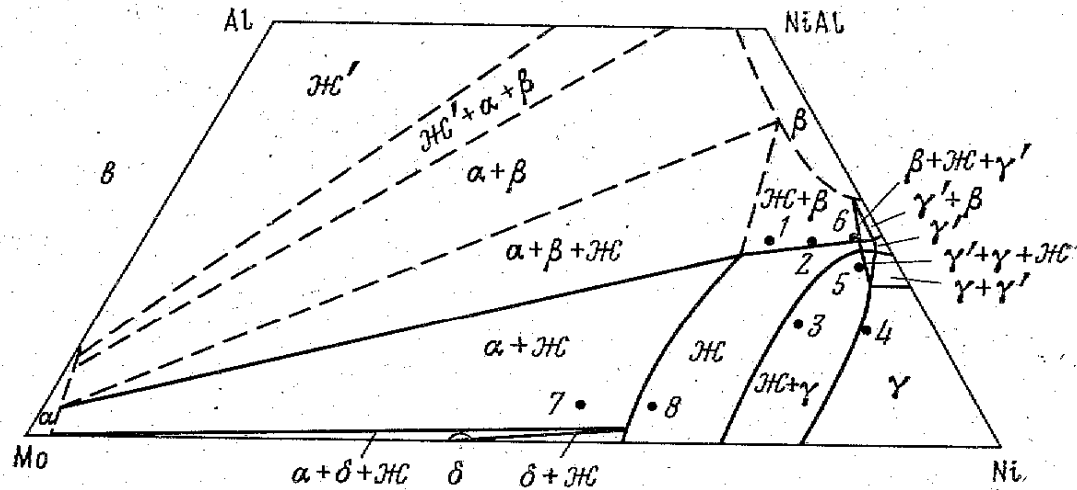


Figure 25. The Ni-Al-Mo ternary phase diagram at 1360 °C by Maslenkov *et al.*

In Figures 23 and 24, there is a distinct change in the liquid shape and volume. The liquid, marked as Ж, was separated by a solid  $\beta + \alpha(\text{Mo})$  two-phase region. The liquid region continues to shrink at 1360 °C, and the solid phase stability increases. As the temperature decreases the  $\gamma-\gamma'$  two-phase region appears and grows. The eutectic temperature in the Ni-Mo binary system is at 1337 °C. Figure 26 shows the phase diagram at 1340 °C. This temperature, just above the eutectic temperature of the binary system shows the presence of the liquid phase. This liquid already exists in equilibrium with the  $\alpha(\text{Mo})$  and  $\gamma'$  phases when it extends to the Ni-Mo binary axis.

Two years later Maslenkov, Burova and Rodimkina<sup>15</sup> furthered their work with four more isothermal sections at 1200, 1100, 880, and 700 °C, Figures 27-30. It can be seen



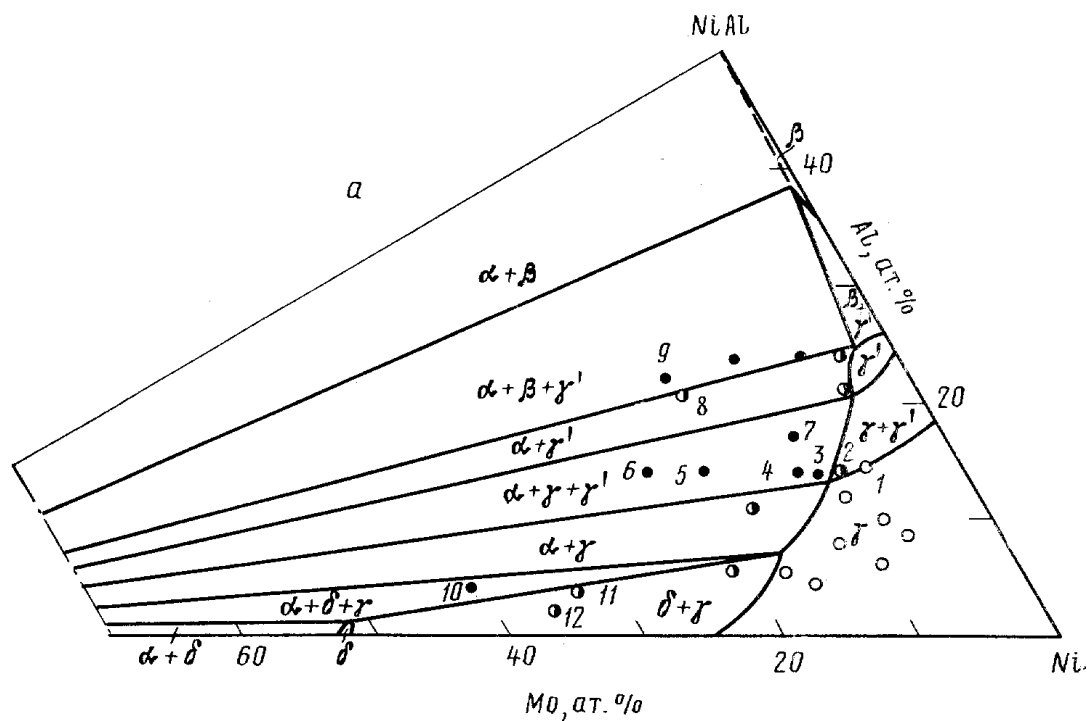


Figure 27. The Ni-Al-Mo ternary phase diagram at 1200 °C by Maslenkov *et al.*

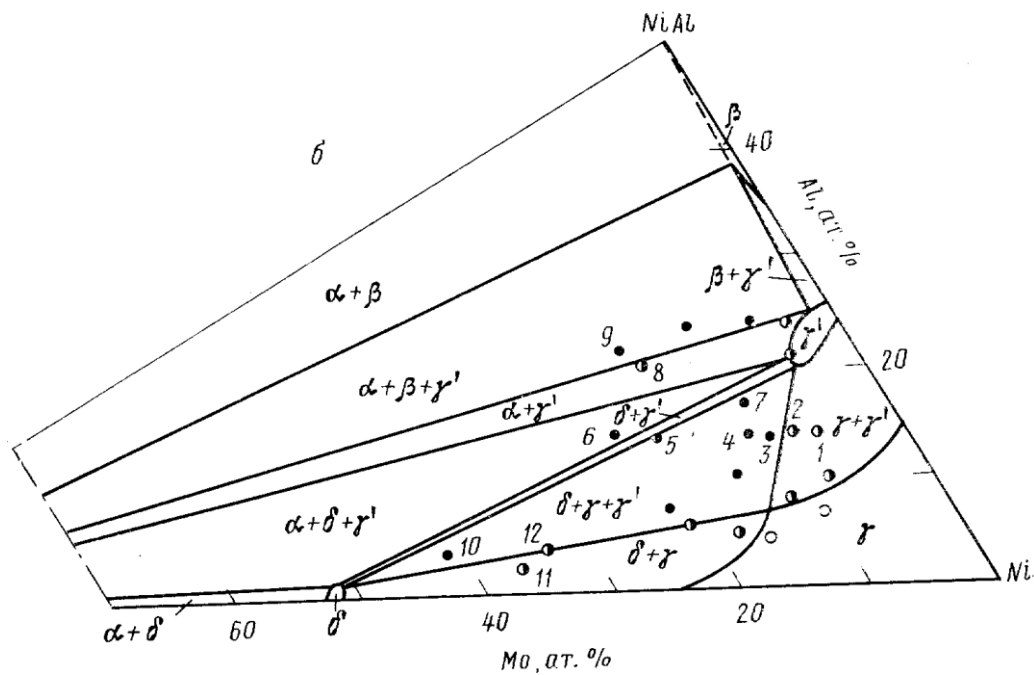


Figure 28. The Ni-Al-Mo ternary phase diagram at 1100 °C by Maslenkov *et al.*

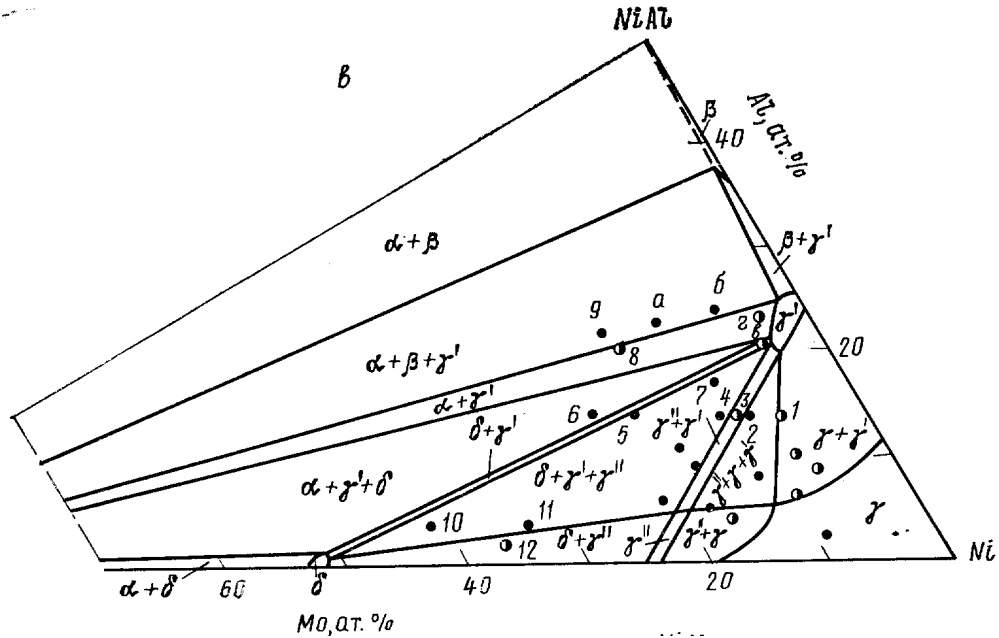


Figure 29. The Ni-Al-Mo ternary phase diagram at 880 °C by Maslenkov *et al.*

In the 1100 °C isothermal section, Figure 28, the solubility limits of the  $\gamma$  have decreased again, which is in agreement with the diagrams from Miracle *et al.* Based on these diagrams, it can be deduced that the  $\gamma + \gamma' + \delta$ -MoNi +  $\alpha$ (Mo) four-phase equilibrium temperature is between 1100 °C and 1171 °C.

At low temperatures in the Ni-Mo binary system there is a second binary phase that can be seen, the  $\gamma''$  ( $\text{Ni}_3\text{Mo}$ ) phase. This phase is not seen in 927 °C phase diagram, Figure 21, because it is not stable at high temperatures. At 700 °C, Figure 30, there is a third binary phase on the Ni-Mo binary system,  $\text{Ni}_4\text{Mo}$ . The solubility of Al and Mo in the  $\gamma$  continues to decrease.



to perform additional experimental work to reduce some of the uncertainty in both the Ni-Al-Cr and Ni-Al-Mo ternary systems.

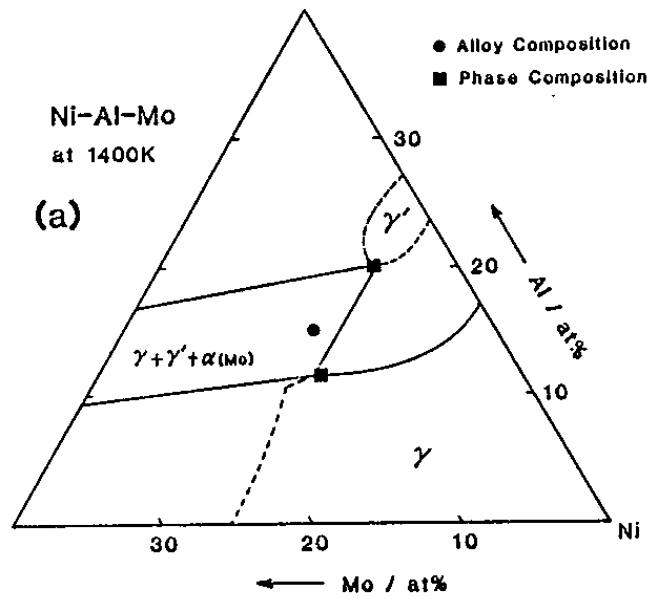


Figure 31. The Ni-rich corner of the Ni-Al-Mo ternary phase diagram at 1400 K by Hong *et al.*

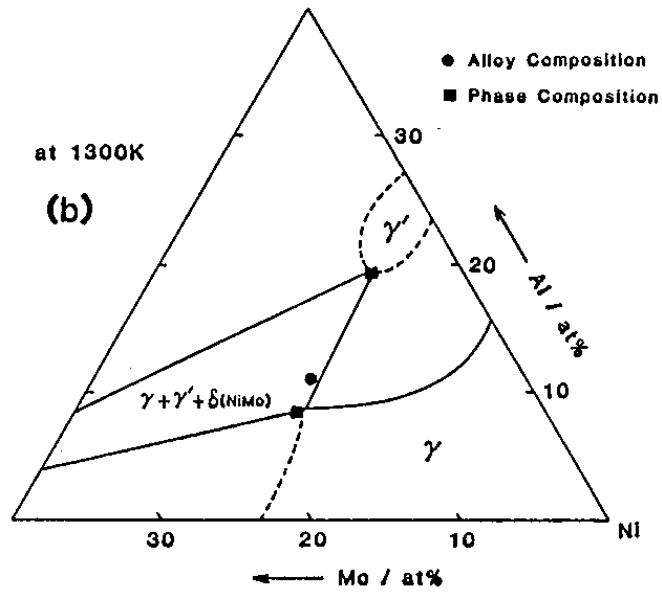


Figure 32. The Ni-rich corner of the Ni-Al-Mo ternary phase diagram at 1300 K by Hong *et al.*

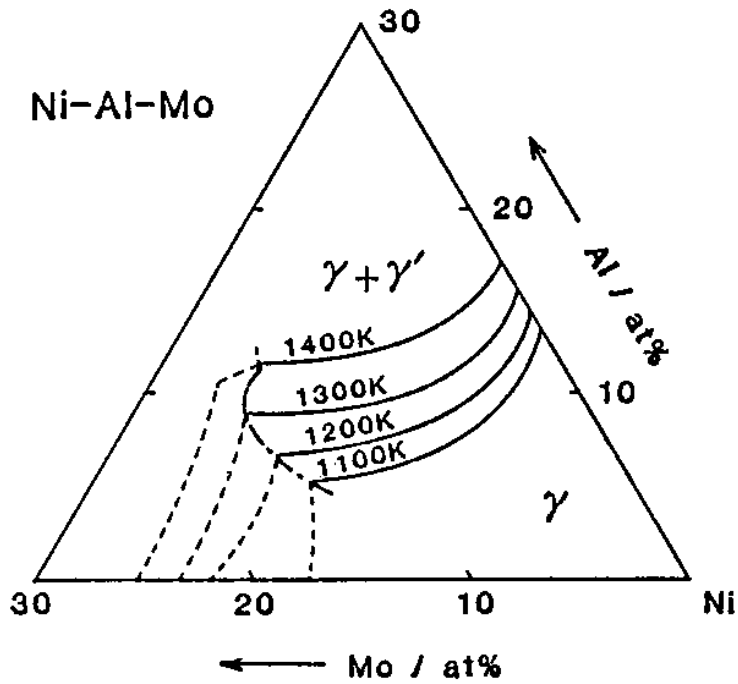


Figure 33. Solvus lines for the  $\gamma'$  phase in the Ni-Al-Mo ternary system by Hong *et al.*

# Experimental Procedure

The diffusion multiples used in this study were produced by Thompson, Zhao and Hemker for their study of the martensitic transformation in  $\beta$ -NiAl<sup>16</sup>. The manufacture of these multiples is detailed in their paper. Each phase diagram reported in the current study was generated from a single ternary region of an individual sample. At the start of this study, the diffusion multiples were re-polished to 0.05 $\mu$ m using colloidal silica. After the polishing, the ternary junctions were mapped using optical microscopes to determine suitable areas for this study. SEM backscatter electron imaging was then performed on the samples. The SEM images were used to mark the locations of the line scans for microprobe analysis. Figure 34 shows the image that was used in the Ni-Al-Cr system. The red lines marked on the interfaces between phases show the line scan positions on this sample. As can be seen in Figure 34, not all of the scans are into single phase regions, and there are voids and pores along the interfaces.

Figure 35 shows an SEM backscatter electron image of the ternary region of the Ni-Al-Mo diffusion multiple. The red lines in this figure also indicate the locations of line scans along the interfaces. Along the interfaces between the Mo and the Ni or the NiAl there are two phase regions. Under normal diffusion conditions in solid state, two-phase regions usually do not exist in binary diffusion couples, but they are allowed for

ternary systems where an extra degree of freedom exists. Nevertheless, some of these two-phase regions may be formed during cooling. Pores and voids can also be seen along the interfaces of this image.

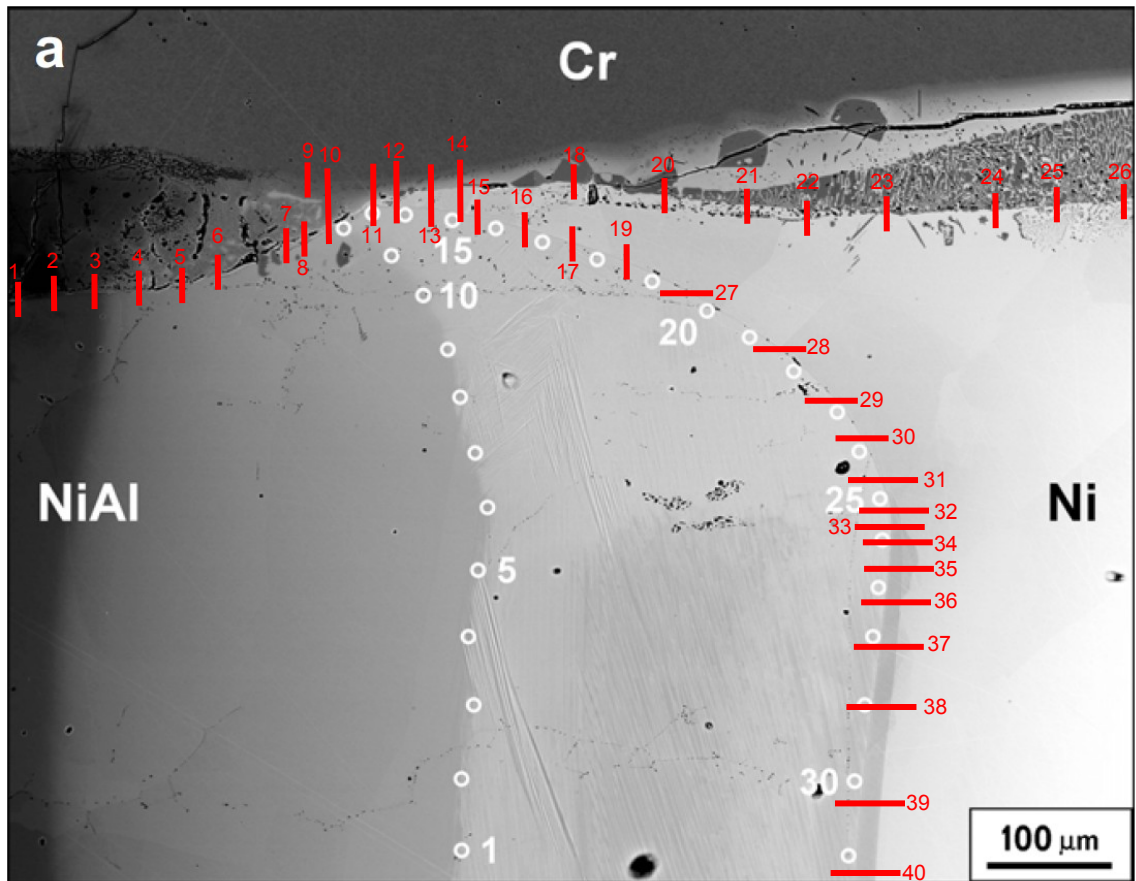


Figure 34. SEM image of the Ni-Al-Cr diffusion multiple used to identify positions for EPMA line scans. The white open circles are for the martensitic transformation and they are unrelated to the current work.

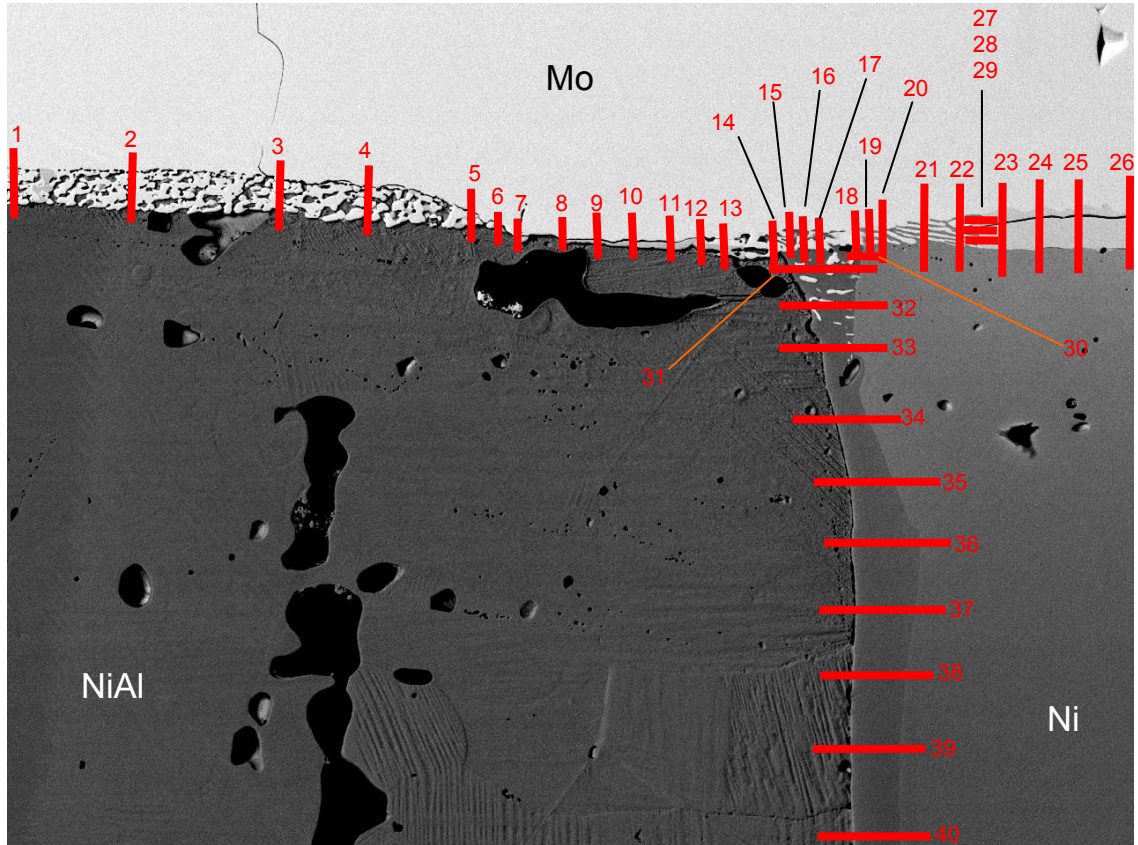


Figure 35. SEM image of the Ni-Al-Mo diffusion multiple used to identify positions for EPMA line scans.

The electron probe microanalysis (EPMA) was performed at the Oregon State University, and the data and samples were then returned to The Ohio State University. All EPMA scans were performed with a 1  $\mu\text{m}$  step size. The microprobe data came in regular cartesian coordinates and both weight percents and atomic percents of each elements. When an EPMA spot hits a pore, the weight percents reported did not add up to 100%. Data points with weight percent total less than 95% were usually discarded. The

rest of the data were normalized. Then the normalized data was transformed using the following equations to plot the data on a triangular plot format that is commonly used for ternary phase diagrams:

$$(Al)_T = (Al)_C + (X)_C \cos\left(\frac{\pi}{3}\right)$$

$$(X)_T = (X)_C \sin\left(\frac{\pi}{3}\right)$$

where X represents the elements Cr or Mo in their respective systems, with the subscript C for the original Cartesian coordinates and the subscript T for the transformed triangular coordinates. With the data now in triangular coordinates, they were plotted all together. The data were then evaluated to determine the phase boundary tie lines. To do this, each line scan was plotted individually both on a triangular plot and on a Cartesian plot against the relative distance of the scan. The phase boundaries were then identified and plotted both with and without the tie lines.

# Results

## **The Ni-Al-Cr Ternary System:**

The results of the experiments are presented in the following figures and tables. Figures 35 and 36 show the data from line scan #15 in the Ni-Al-Cr system. In Figure 35 there is a distinct jump of the concentrations of the Al and the Mo at the 12  $\mu\text{m}$  scan position, which corresponds to a change in phase, from the  $\beta$ -NiAl phase to the  $\gamma$  (Ni) phase.

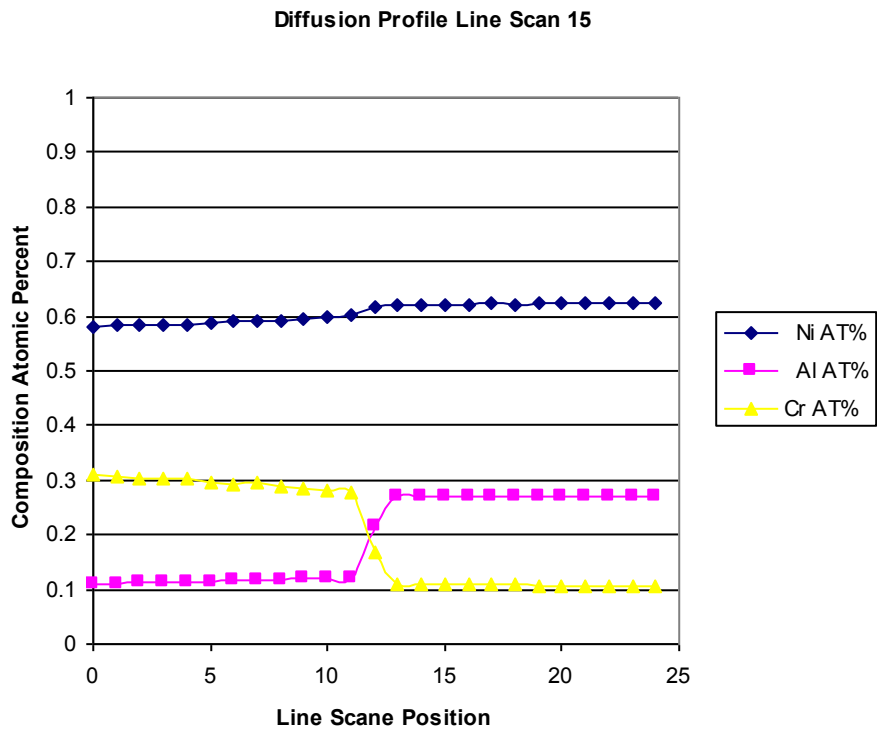


Figure 36. EPMA results for line scan #15 on the Ni-Al-Cr diffusion multiple at 1200 °C showing composition vs. relative distance of the scan.

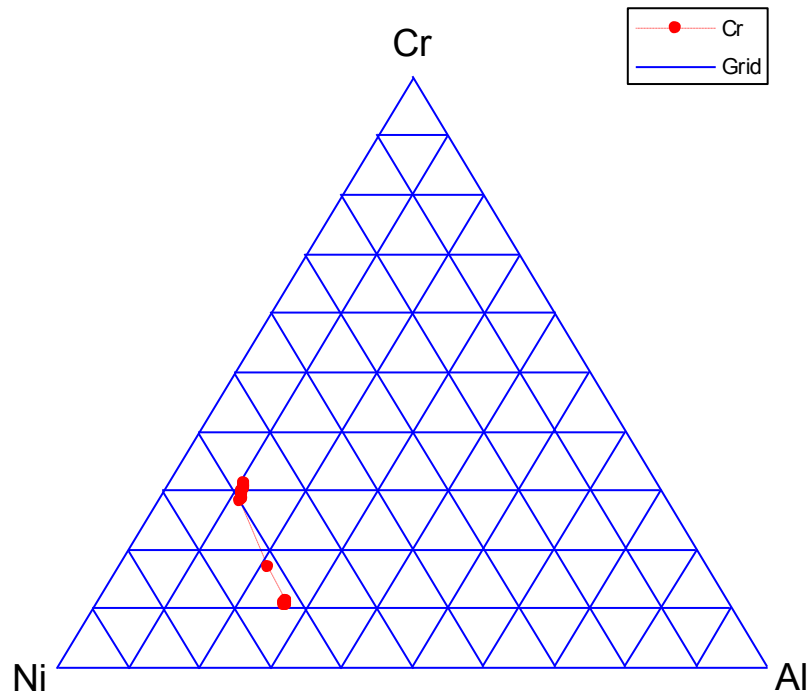


Figure 37. EPMA results for line scan #15 on the Ni-Al-Cr diffusion multiple at 1200 °C in a triangular composition vs. composition plot (Data are plotted in at.% axes. The lower left corner is Ni, lower right is Al, and top is Cr).

There is one point at the 12  $\mu\text{m}$  position that appears to be between the two phases. Figure 37 is a plot of the data in a triangular plot that is commonly for with ternary phase diagrams. It can be seen that the point lies on the tie-line between the  $\gamma(\text{Ni})$  phase and the  $\beta\text{-NiAl}$  phase, indicating that the EPMA point was at the phase interface, thus sampling both phases at the same time. By utilizing this method of data analysis, the following results were produced and are recorded in Tables 1.

Table 1 Phase boundary results from the EPMA analysis of the Ni-Al-Cr diffusion multiple.

		Measured Concentration					Measured Concentration		
Scan	Phase	Ni	Al	Cr	Scan	Phase	Ni	Al	Cr
1	$\alpha(\text{Cr})$	0.026	0.273	0.701	28	$\gamma(\text{Ni})$	0.679	0.154	0.167
	NiAl	0.527	0.445	0.029		NiAl	0.658	0.272	0.070
2	$\alpha(\text{Cr})$	0.032	0.278	0.690	29	$\gamma(\text{Ni})$	0.701	0.162	0.137
	NiAl	0.524	0.446	0.030		NiAl	0.667	0.275	0.058
3	$\alpha(\text{Cr})$	0.039	0.261	0.700	30	$\gamma(\text{Ni})$	0.712	0.172	0.116
	NiAl	0.525	0.443	0.032		NiAl	0.672	0.275	0.052
4	$\alpha(\text{Cr})$	0.030	0.251	0.719	31	$\gamma(\text{Ni})$	0.718	0.167	0.114
	NiAl	0.531	0.434	0.035		NiAl	0.679	0.272	0.049
5	$\alpha(\text{Cr})$	0.024	0.182	0.793	32	$\gamma(\text{Ni})$	0.740	0.161	0.098
	NiAl	0.550	0.423	0.028		$\text{Ni}_3\text{Al} (1)$	0.745	0.200	0.055
6	$\alpha(\text{Cr})$	0.061	0.014	0.926		$\text{Ni}_3\text{Al} (2)$	0.737	0.207	0.056
	NiAl	0.580	0.319	0.100	NiAl	0.676	0.278	0.046	
7	$\alpha(\text{Cr})$	0.111	0.012	0.877	33	$\gamma(\text{Ni})$	0.750	0.159	0.091
	NiAl	0.592	0.278	0.130		$\text{Ni}_3\text{Al} (1)$	0.750	0.198	0.051
8	$\alpha(\text{Cr})$	0.127	0.014	0.859		$\text{Ni}_3\text{Al} (2)$	0.739	0.208	0.052
	NiAl	0.600	0.279	0.121	NiAl	0.678	0.277	0.045	
10	$\alpha(\text{Cr})$	0.164	0.016	0.820	34	$\gamma(\text{Ni})$	0.759	0.157	0.083
	NiAl	0.594	0.275	0.131		$\text{Ni}_3\text{Al} (1)$	0.756	0.195	0.049
11	$\alpha(\text{Cr})$	0.181	0.019	0.800		$\text{Ni}_3\text{Al} (2)$	0.741	0.207	0.052
	$\gamma(\text{Ni}) (1)$	0.550	0.105	0.345	NiAl	0.679	0.281	0.042	
	$\gamma(\text{Ni}) (2)$	0.558	0.108	0.334	35	$\gamma(\text{Ni})$	0.764	0.159	0.077
	NiAl	0.601	0.265	0.134		$\text{Ni}_3\text{Al} (1)$	0.758	0.196	0.046
12	$\alpha(\text{Cr})$	0.184	0.020	0.796	$\text{Ni}_3\text{Al} (2)$	0.739	0.213	0.049	
	$\gamma(\text{Ni}) (1)$	0.539	0.109	0.352	NiAl	0.686	0.274	0.040	
	$\gamma(\text{Ni}) (2)$	0.571	0.116	0.313	36	$\gamma(\text{Ni})$	0.770	0.158	0.072
	NiAl	0.605	0.267	0.128		$\text{Ni}_3\text{Al} (1)$	0.760	0.196	0.043
13	$\alpha(\text{Cr})$	0.176	0.017	0.806		$\text{Ni}_3\text{Al} (2)$	0.743	0.211	0.046
	$\gamma(\text{Ni}) (1)$	0.535	0.097	0.368	NiAl	0.680	0.280	0.039	
	$\gamma(\text{Ni}) (2)$	0.585	0.122	0.293	37	$\gamma(\text{Ni})$	0.781	0.160	0.059
	NiAl	0.611	0.268	0.122		$\text{Ni}_3\text{Al} (1)$	0.767	0.195	0.038
14	$\alpha(\text{Cr})$	0.189	0.017	0.794		$\text{Ni}_3\text{Al} (2)$	0.744	0.216	0.040
	$\gamma(\text{Ni}) (1)$	0.535	0.089	0.377	NiAl	0.680	0.283	0.035	
	$\gamma(\text{Ni}) (2)$	0.592	0.116	0.292	38	$\gamma(\text{Ni})$	0.793	0.161	0.046
	NiAl	0.617	0.265	0.118		$\text{Ni}_3\text{Al} (1)$	0.774	0.194	0.032

Continued

Table 1 Continued

15	NiAl	0.620	0.270	0.110		Ni <sub>3</sub> Al (2)	0.747	0.220	0.034
	$\gamma$ (Ni)	0.601	0.121	0.279		NiAl	0.683	0.286	0.031
16	$\gamma$ (Ni)	0.613	0.262	0.125		$\gamma$ (Ni)	0.814	0.164	0.022
	NiAl	0.629	0.267	0.104		Ni <sub>3</sub> Al (1)	0.781	0.204	0.015
17	$\gamma$ (Ni)	0.630	0.135	0.235	39	Ni <sub>3</sub> Al (2)	0.752	0.230	0.018
	NiAl	0.636	0.261	0.103		NiAl	0.690	0.293	0.017
19	$\gamma$ (Ni)	0.643	0.134	0.223		$\gamma$ (Ni)	0.823	0.164	0.013
	NiAl	0.642	0.270	0.087		Ni <sub>3</sub> Al (1)	0.785	0.205	0.010
21	$\alpha$ (Cr)	0.262	0.010	0.728	40	Ni <sub>3</sub> Al (2)	0.754	0.233	0.013
	$\gamma$ (Ni)	0.574	0.070	0.356		NiAl	0.691	0.297	0.012
27	$\gamma$ (Ni)	0.660	0.140	0.200					
	NiAl	0.650	0.272	0.078					

Table 1 details all of the data points that are included in the isotherm at 1200 °C for the Ni-Al-Cr system. Each of these points has a corresponding point across a tie line. Figure 38 shows the data for the Ni-Al-Cr system with the tie-lines that were measured in the experiment. Two three-phase regions are visible. These three-phase regions are  $\gamma$ (Ni) +  $\gamma'$ -Ni<sub>3</sub>Al +  $\beta$ -NiAl and  $\gamma$ (Ni) +  $\beta$ -NiAl +  $\alpha$ (Cr). The corners of these three phase regions can be seen in Tables 2 and 3. The data in these tables were used to mark the three-phase regions on the phase diagrams, Figures 39 and 40 with Figure 40 being an expanded view of the Ni-rich corner. The phase boundaries in Figures 39 and 40 were drawn by hand with consideration of the Gibbs phase rule and a consistency with the binary phase diagrams.

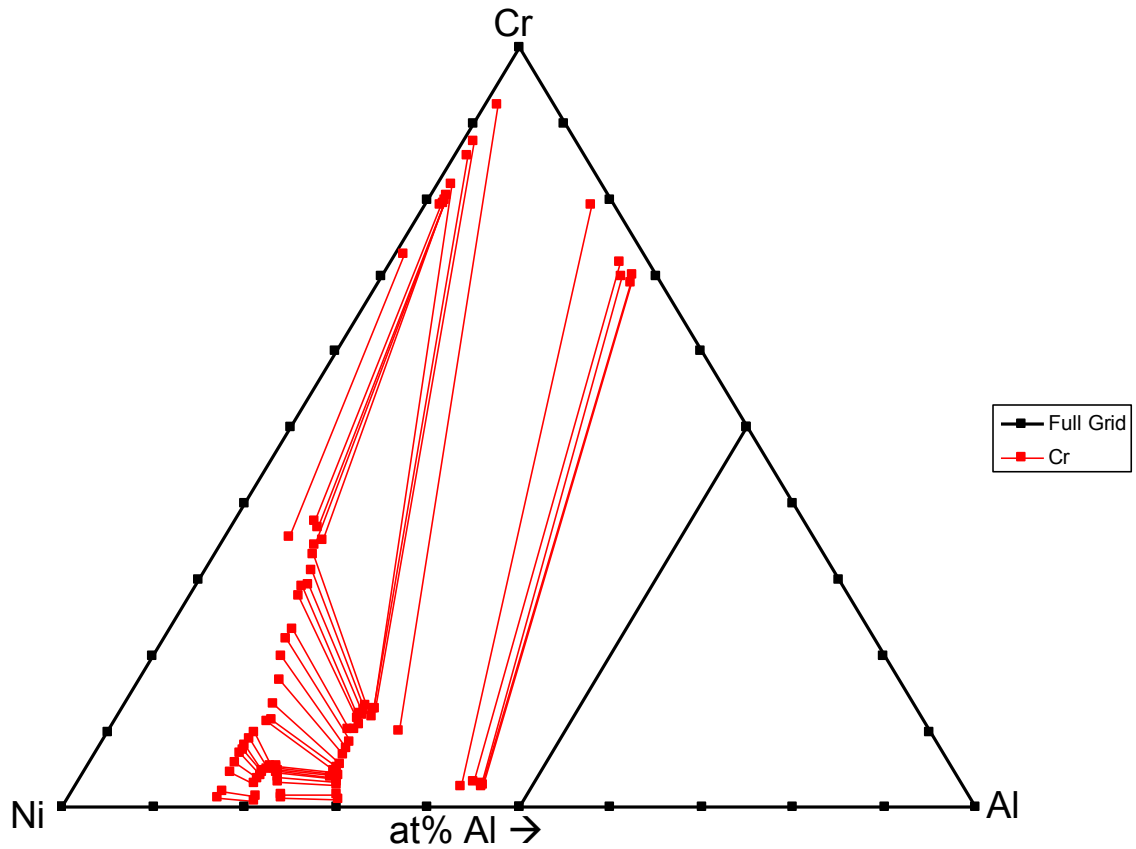


Figure 38. Tie lines for the Ni-Al-Cr ternary phase diagram at 1200 °C.

Table 2. Three-phase equilibrium among the  $\gamma$ - $\beta$ - $\alpha(\text{Cr})$  phases.

Phase	Ni	Al	Cr
$\gamma$	0.5388	0.1091	0.3522
$\beta$	0.5962	0.2692	0.1346
$\alpha(\text{Cr})$	0.1731	0.02	0.8069

Table 3. Three-phase equilibrium among the  $\gamma$ - $\gamma'$ - $\beta$  phases.

Phase	Ni	Al	Cr
$\gamma$	0.7185	0.167	0.1141
$\gamma'$	0.7385	0.2038	0.0577
$\beta$	0.6791	0.2722	0.0487

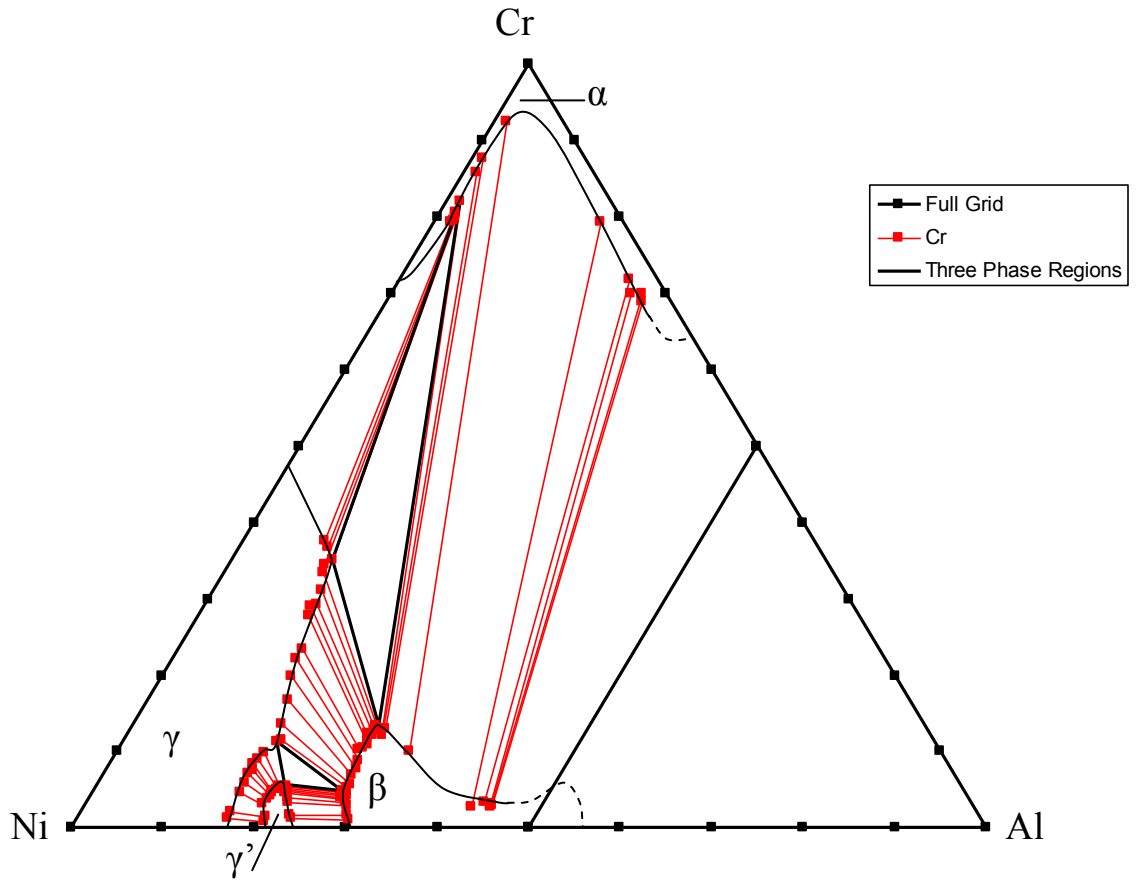


Figure 39. The Ni-Al-Cr ternary phase diagram at 1200 °C.

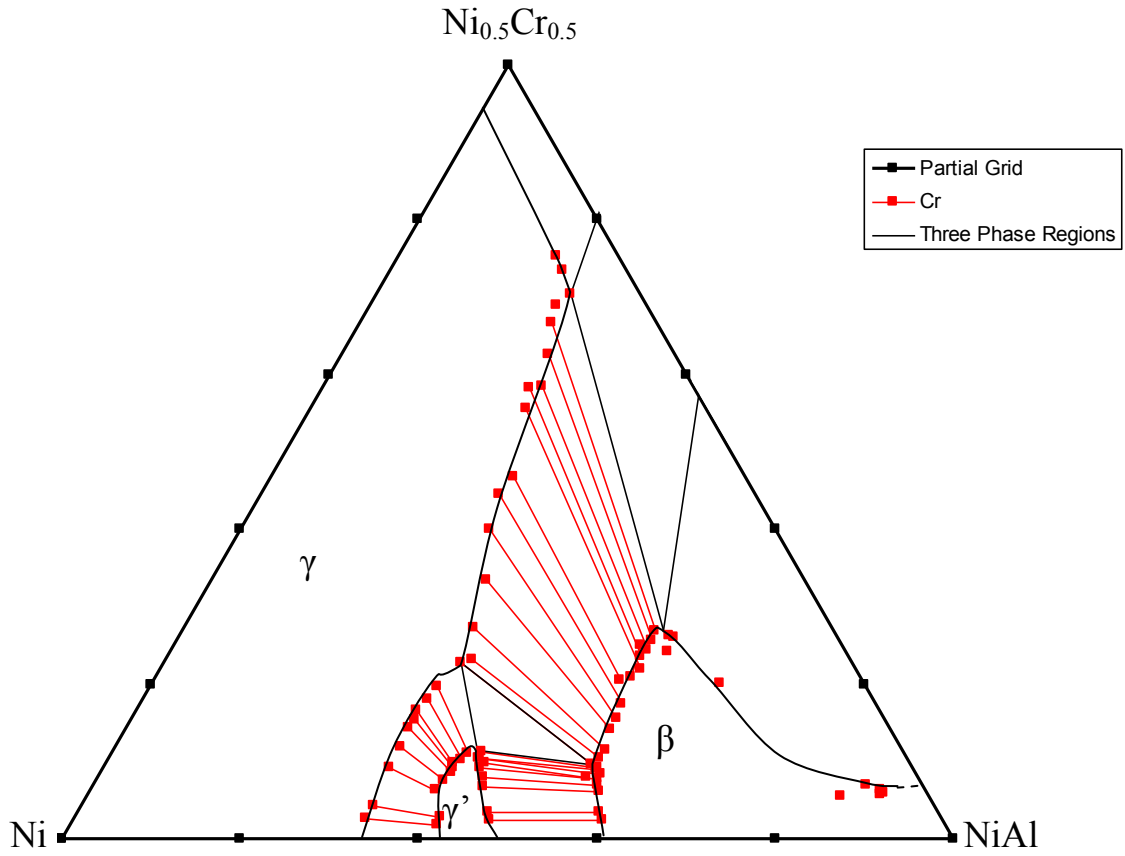


Figure 40. The Ni-rich corner of the Ni-Al-Cr ternary phase diagram at 1200 °C.

### **The Ni-Al-Mo Ternary System:**

The Ni-Al-Mo system was studied in a similar manner to establish an isothermal section at 1200 °C. A similar set of line scans was employed for EPMA in the Ni-Al-Mo system and the results were analyzed by plotting them. Figure 41 shows a plot of line scan #10. In this line scan, three phases have been measured:  $\beta$ -NiAl,  $\text{Ni}_5\text{Al}_2\text{Mo}_8$  and  $\alpha(\text{Mo})$ . There are also points on the plot that likely indicate the EPMA points were on

the phase interfaces, thus sampling both phases at the same time. In the corresponding triangular plot (Figure 42), the three phases are very clearly seen.

Figures 41 and 42 also provide evidence for the existence of the  $\text{Ni}_5\text{Al}_2\text{Mo}_8$  phase. In Figure 41, there is a succession of four points that exhibit linear behavior at a composition that is neither the  $\gamma(\text{Ni})$  phase nor the  $\alpha(\text{Mo})$  phase. In Figure 42 the four points are shown to be clustered together the way that other phases are, and are in a location that is not connected to any known phases in the phase diagram.

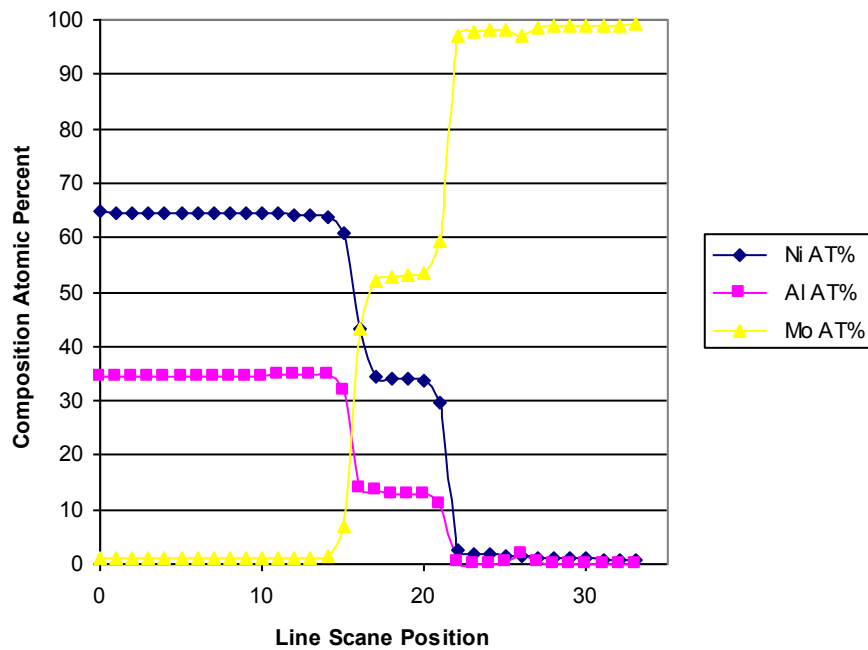


Figure 41. EPMA results for line scan # 10 on the Ni-Al-Mo diffusion multiple at 1200 °C showing composition vs relative distance of the line scan.

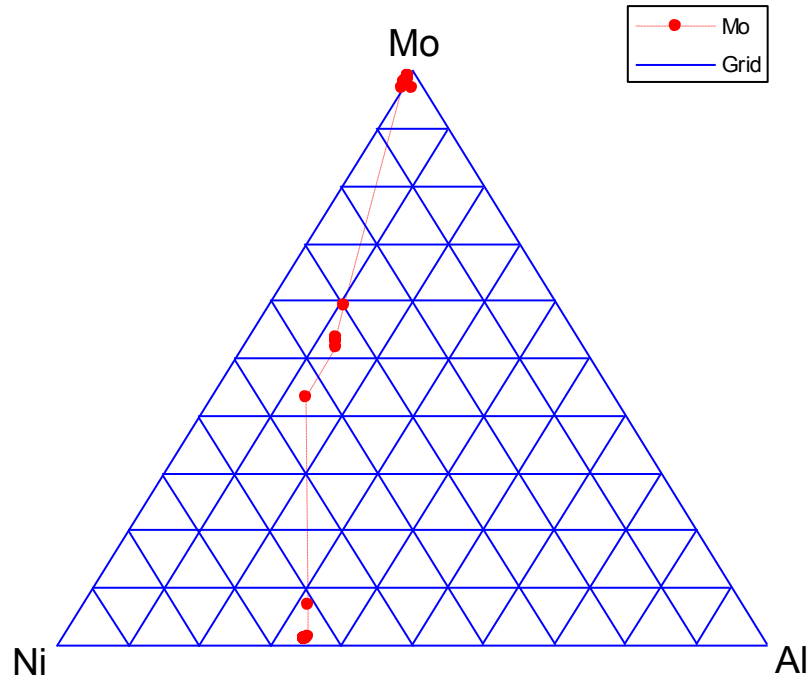


Figure 42. EPMA results for line scan # 10 on the Ni-Al-Mo diffusion multiple at 1200 C in a triangular composition vs. composition plot (Data are plotted in at.% axes. The lower left corner is Ni, lower right is Al, and top is Mo)

The same procedure was applied for each of the line scans in the system. Not every scan produced useable results. The  $\text{Ni}_5\text{Al}_2\text{Mo}_8$  phase was present in four scans. The presence of the  $\text{Ni}_5\text{Al}_2\text{Mo}_8$  phase in multiple scans is a further argument towards the existence of this phase. The useable data from these scans is listed in Table 4. Each set of two distinct phases within a scan forms the end points of a tie line that follows the phase boundaries.

Table 4 Phase boundary results from EPMA analysis of the Ni-Al-Mo diffusion multiple.

		Measured Concentration					Measured Concentration		
Scan	Phase	Ni	Al	Cr	Scan	Phase	Ni	Al	Cr
4	$\alpha(\text{Mo})$	0.025	0.013	0.961	26	$\alpha(\text{Mo})$	0.018	0.000	0.982
	$\gamma(\text{Ni})$	0.631	0.361	0.008		MoNi (1)	0.470	0.006	0.524
5	$\alpha(\text{Mo})$	0.012	0.008	0.972		MoNi (2)	0.515	0.009	0.476
	$\gamma(\text{Ni})$	0.634	0.356	0.010	$\gamma(\text{Ni})$	0.737	0.041	0.221	
6	$\alpha(\text{Mo})$	0.024	0.003	0.973	28	MoNi	0.481	0.016	0.503
	$\gamma(\text{Ni})$	0.639	0.352	0.009		$\gamma(\text{Ni})$	0.719	0.100	0.181
10	$\gamma(\text{Ni})$	0.637	0.347	0.015	29	MoNi	0.485	0.017	0.498
	$\text{Ni}_5\text{Al}_2\text{Mo}_8$ (1)	0.346	0.134	0.520		$\gamma(\text{Ni})$	0.732	0.102	0.166
	$\text{Ni}_5\text{Al}_2\text{Mo}_8$ (1)	0.337	0.128	0.535	30	$\gamma(\text{Ni})$	0.717	0.151	0.132
	$\alpha(\text{Mo})$	0.027	0.002	0.971		$\text{Ni}_3\text{Al}$	0.733	0.212	0.055
12	$\gamma(\text{Ni})$	0.639	0.349	0.015	31	NiAl	0.644	0.347	0.009
	$\text{Ni}_5\text{Al}_2\text{Mo}_8$ (1)	0.340	0.130	0.530		$\text{Ni}_3\text{Al}$	0.726	0.248	0.026
	$\text{Ni}_5\text{Al}_2\text{Mo}_8$ (1)	0.333	0.127	0.540	32	$\gamma(\text{Ni})$	0.731	0.151	0.118
	$\alpha(\text{Mo})$	0.018	0.001	0.980		$\text{Ni}_3\text{Al}$	0.741	0.215	0.044
13	$\gamma(\text{Ni})$	0.643	0.344	0.013	33	$\gamma(\text{Ni})$	0.739	0.150	0.112
	$\text{Ni}_5\text{Al}_2\text{Mo}_8$ (1)	0.346	0.127	0.528		$\text{Ni}_3\text{Al}$ (1)	0.744	0.206	0.050
	$\text{Ni}_5\text{Al}_2\text{Mo}_8$ (1)	0.334	0.125	0.540		$\text{Ni}_3\text{Al}$ (2)	0.726	0.250	0.024
	$\alpha(\text{Mo})$	0.015	0.001	0.984		NiAl	0.643	0.349	0.008
16	$\alpha(\text{Mo})$	0.033	0.003	0.964	35	$\gamma(\text{Ni})$	0.755	0.146	0.098
	$\gamma(\text{Ni})$	0.729	0.238	0.032		$\text{Ni}_3\text{Al}$ (1)	0.750	0.206	0.046
19	$\alpha(\text{Mo})$	0.035	0.005	0.959		$\text{Ni}_3\text{Al}$ (2)	0.729	0.248	0.023
	$\gamma(\text{Ni})$	0.733	0.143	0.123	NiAl	0.647	0.346	0.007	
20	$\alpha(\text{Mo})$	0.012	0.002	0.986	36	$\gamma(\text{Ni})$	0.755	0.146	0.098
	$\gamma(\text{Ni})$	0.736	0.135	0.130		$\text{Ni}_3\text{Al}$ (1)	0.748	0.206	0.046
21	$\alpha(\text{Mo})$	0.018	0.000	0.982		$\text{Ni}_3\text{Al}$ (2)	0.722	0.256	0.021
	$\gamma(\text{Ni})$	0.735	0.128	0.137		NiAl	0.647	0.346	0.007
22	$\alpha(\text{Mo})$	0.026	0.001	0.973	37	$\gamma(\text{Ni})$	0.801	0.161	0.038
	$\gamma(\text{Ni})$	0.735	0.120	0.145		$\text{Ni}_3\text{Al}$ (1)	0.764	0.207	0.029
23	$\alpha(\text{Mo})$	0.018	0.000	0.982		$\text{Ni}_3\text{Al}$ (2)	0.724	0.257	0.019
	MoNi (1)	0.475	0.011	0.513	NiAl	0.649	0.345	0.006	
	MoNi (2)	0.495	0.012	0.493	38	$\gamma(\text{Ni})$	0.807	0.173	0.019
	$\gamma(\text{Ni})$	0.737	0.073	0.191		$\text{Ni}_3\text{Al}$ (1)	0.768	0.212	0.020
$\alpha(\text{Mo})$	0.023	0.001	0.976	$\text{Ni}_3\text{Al}$ (2)		0.727	0.253	0.020	
24	MoNi (1)	0.478	0.010	0.512	NiAl	0.646	0.349	0.006	
	MoNi (2)	0.500	0.010	0.490	39	$\gamma(\text{Ni})$	0.809	0.181	0.010
	$\gamma(\text{Ni})$	0.734	0.062	0.204		$\text{Ni}_3\text{Al}$ (1)	0.765	0.222	0.012
	$\alpha(\text{Mo})$	0.015	0.000	0.985		$\text{Ni}_3\text{Al}$ (2)	0.730	0.251	0.019
25	MoNi (1)	0.480	0.007	0.513	NiAl	0.645	0.351	0.004	
	MoNi (2)	0.502	0.010	0.489	40	$\gamma(\text{Ni})$	0.802	0.192	0.006
	$\gamma(\text{Ni})$	0.739	0.051	0.210		$\text{Ni}_3\text{Al}$ (1)	0.767	0.226	0.008
						$\text{Ni}_3\text{Al}$ (2)	0.727	0.256	0.017
				NiAl	0.647	0.350	0.004		

Figure 43 shows the data and tie-lines for the Ni-Al-Mo system plotted together on a triangular plot. There are three three-phase regions that seen in the plot, along with two that must be there due to the Gibbs phase rule, but that do not have data confirming their existence at this time.

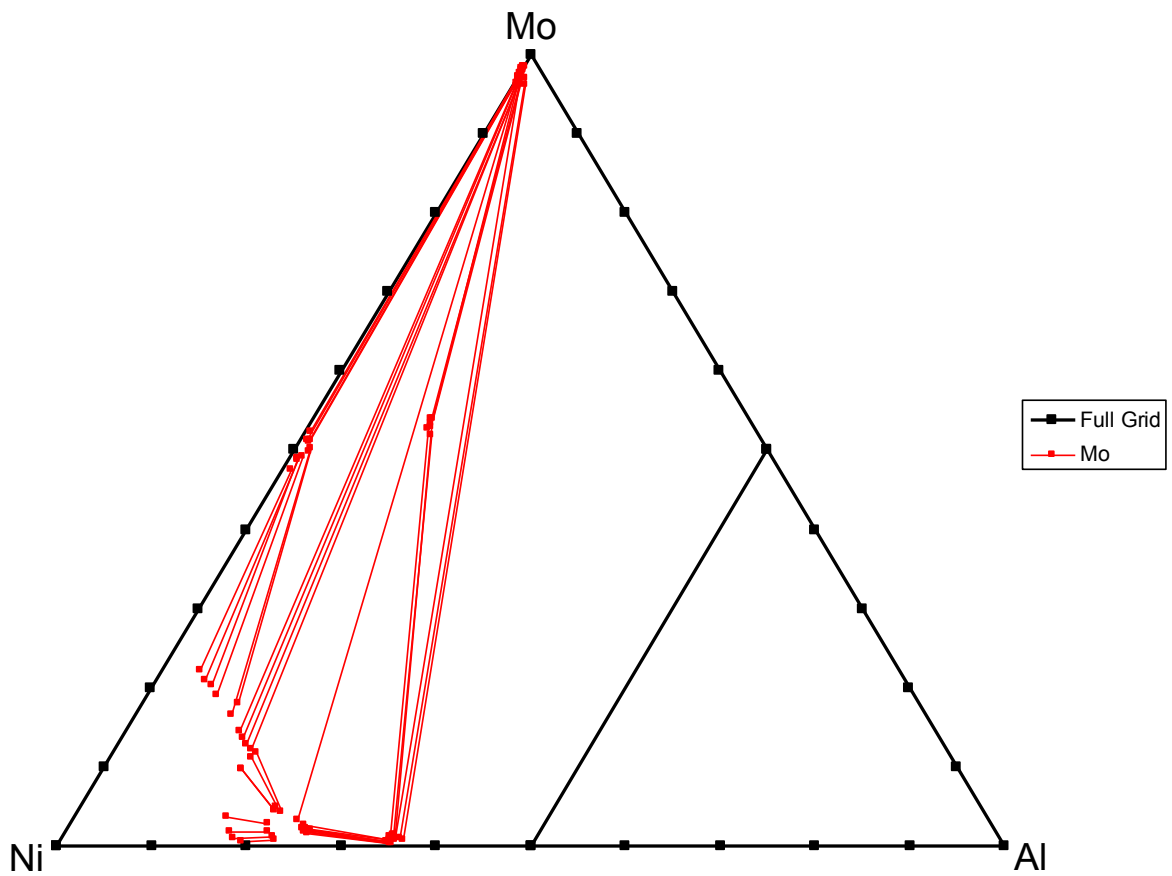


Figure 39. Tie lines for the Ni-Al-Mo ternary phase diagram at 1200 °C.

Tables 5, 6, and 7 report the data for the three-phase regions that can be confirmed by Figure 43. These tables follow the same format that is seen in Table 4. They start with left side of the diagram in the  $\gamma(\text{Ni}) + \delta\text{-NiMo} + \alpha(\text{Mo})$  three-phase region and move to the right to end with the  $\beta\text{-NiAl} + \text{Ni}_5\text{Al}_2\text{Mo}_8 + \alpha(\text{Mo})$  three-phase region.

Table 5. Three-phase region among the  $\gamma\text{-}\delta\text{-}\alpha(\text{Mo})$  phases.

Phase	Ni	Al	Mo
$\gamma$	0.725	0.1094	0.1656
$\delta$	0.4847	0.0168	0.4985
$\alpha(\text{Mo})$	0.0375	0.0016	0.9609

Table 6. Three-phase region among the  $\gamma\text{-}\gamma'\text{-}\alpha(\text{Mo})$  phases.

Phase	Ni	Al	Mo
$\gamma$	0.7273	0.1545	0.1182
$\gamma'$	0.7409	0.215	0.0441
$\alpha(\text{Mo})$	0.0375	0.0031	0.9594

Table 7. Three-phase region among the  $\beta\text{-Ni}_5\text{Al}_2\text{Mo}_8\text{-}\alpha(\text{Mo})$  phases.

Phase	Ni	Al	Mo
$\beta$	0.6333	0.348	0.0187
$\text{Ni}_5\text{Al}_2\text{Mo}_8$	0.3401	0.1301	0.5298
$\alpha(\text{Mo})$	0.0312	0.0094	0.9594

The three-phase regions that are reported in Tables 8 and 9 do not appear in their entirety in the results of this experiment. However, they are proposed because of the

shapes of the phase boundaries in Figure 43. There is one tie line between the  $\gamma'$  and  $\alpha(\text{Mo})$  phases indicating a stability between the two phases. Because of this, there must be a three-phase region that transitions from that two-phase region to the  $\text{Ni}_5\text{Al}_2\text{Mo}_8$  phase as shown in Table 8. Table 9 contains the three-phase region between the  $\gamma'$ ,  $\beta$ , and  $\text{Ni}_5\text{Al}_2\text{Mo}_8$ . This is shown because there is a three-phase region between the  $\gamma'$ ,  $\text{Ni}_5\text{Al}_2\text{Mo}_8$  and  $\alpha(\text{Mo})$  that has been postulated and there is three-phase region between  $\beta$ ,  $\text{Ni}_5\text{Al}_2\text{Mo}_8$  and  $\alpha(\text{Mo})$  that is seen in Figure 43. The existence of both of these three-phase regions shows that there must be another three phase region below the  $\text{Ni}_5\text{Al}_2\text{Mo}_8$  phase, among the  $\gamma'$ ,  $\beta$ , and  $\text{Ni}_5\text{Al}_2\text{Mo}_8$  phases.

Table 8. Three-phase region among the  $\gamma'$ - $\text{Ni}_5\text{Al}_2\text{Mo}_8$ - $\alpha(\text{Mo})$  phases.

Phase	Ni	Al	Mo
$\gamma'$	0.7293	0.2384	0.0323
$\text{Ni}_5\text{Al}_2\text{Mo}_8$	0.3521	0.12	0.5279
$\alpha(\text{Mo})$	0.0344	0.0047	0.9609

Table 9. Three-phase region among the  $\gamma'$ - $\beta$ - $\text{Ni}_5\text{Al}_2\text{Mo}_8$  phases.

Phase	Ni	Al	Mo
$\gamma'$	0.7291	0.2476	0.0233
$\beta$	0.6473	0.346	0.0067
$\text{Ni}_5\text{Al}_2\text{Mo}_8$	0.3525	0.13	0.5175

All these information are summarized on the 1200 °C isothermal sections of the Ni-Al-Mo ternary system shown in Figures 44 and 45 with Figure 45 being an expanded view of the Ni-rich corner. The most noteworthy feature of Figure 44 is the existence of the new phase,  $\text{Ni}_5\text{Al}_2\text{Mo}_8$ . This phase did not appear in any previously reported isotherm. The solubility of Mo in the  $\beta$ -NiAl phase is much less than the solubility of Cr. Consequently there is not a three-phase region that involves both  $\gamma$  and  $\beta$ . The three-phase regions that are observed are the  $\gamma + \delta + \alpha(\text{Mo})$ ,  $\gamma + \gamma' + \alpha(\text{Mo})$ , and  $\beta\text{-NiAl} + \text{Ni}_5\text{Al}_2\text{Mo}_8 + \alpha(\text{Mo})$ . The three-phase regions of  $\gamma' + \text{Ni}_5\text{Al}_2\text{Mo}_8 + \alpha(\text{Mo})$ , and  $\gamma' + \beta\text{-NiAl} + \text{Ni}_5\text{Al}_2\text{Mo}_8$  are proposed from the positions of the phases and the tie-lines that have been observed. The Mo solubility in the  $\gamma'$  is also less than that of Cr. The  $\beta$  phase would extend further towards the Al-rich corner of the phase diagram if there were data from the experiment that covered that composition range.

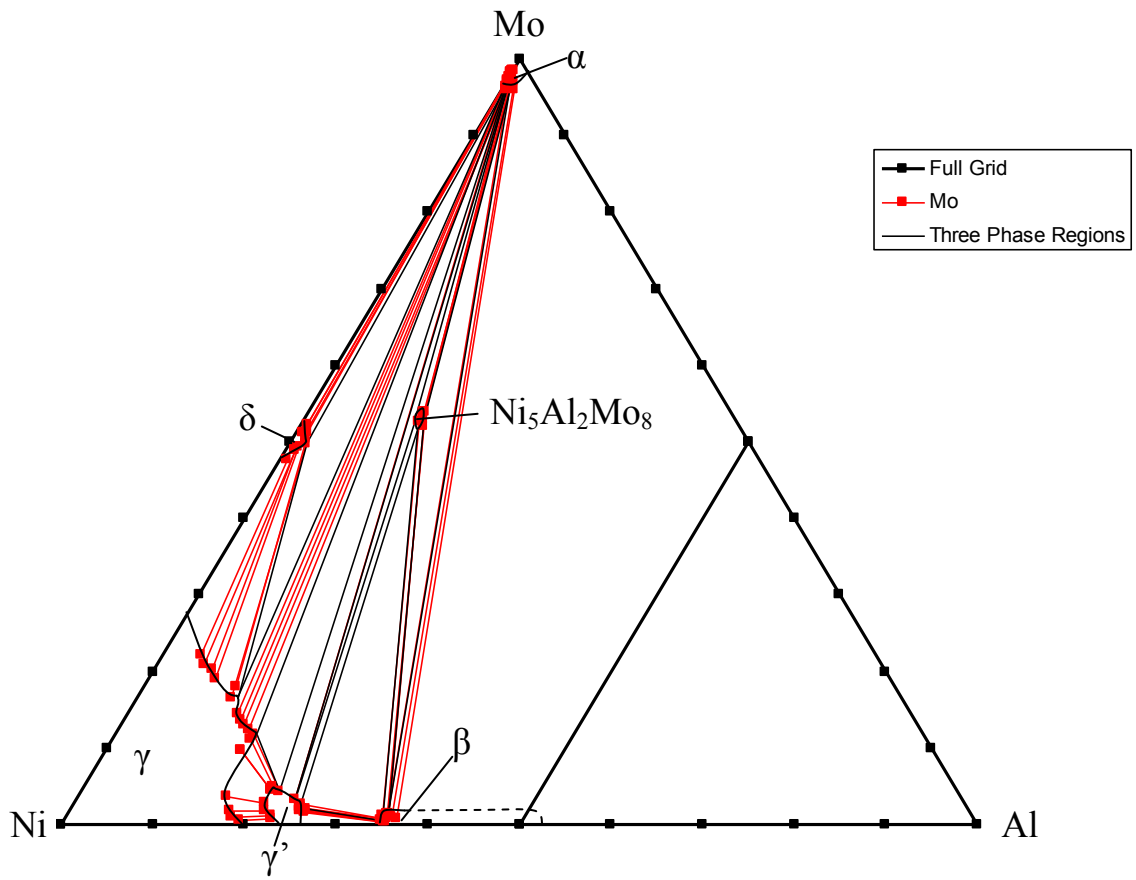


Figure 40. The Ni-Al-Mo ternary phase diagram at 1200 °C.

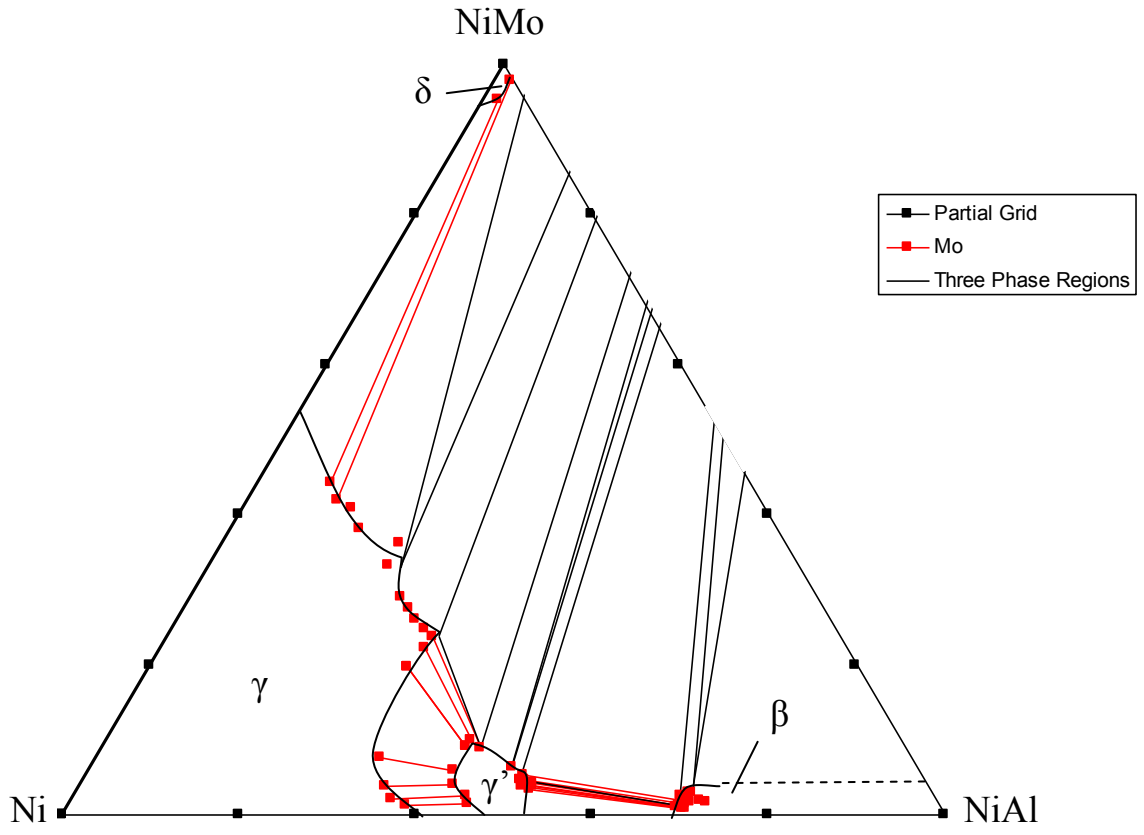


Figure 41. The Ni-rich corner of the Ni-Al-Mo ternary phase diagram at 1200 °C.

# Discussion

## The Ni-Al-Cr Ternary System:

The shape of the  $\alpha(\text{Cr})$  phase region in the Ni-Al-Cr ternary system observed in the current study (Figure 39) is also much different from what was previously reported in literature. The phase region was normally reported just a triangle linking the binary Cr-Ni system to the Cr-Al system, with much higher solubility of Al than of Ni (Figures 8, 9 and 15). The current study found that the  $\alpha(\text{Cr})$  phase region has an overall shape like a 90° corner plate or horseshoe, i.e., high Ni solubility was only observed when the Al solubility is less than ~3 at.% and similarly high Al solubility was only observed when the Ni solubility is less than ~3 at.%. There is no region where both high solubility of Ni and Al can be observed.

Since there are no 1200 °C isothermal sections of the Ni-Al-Cr ternary system in the literature for a direct comparison with the results from the current study. The newly determined 1200 °C section (Figure 39) is compared with Figures 9 and 15, both at 1150 °C. In the  $\alpha(\text{Cr})$  phase the expected solubility based on the binary phase diagram (Figure 4) at 1150 °C is ~22 at% Ni, and at 1200 °C it is 28 at% Ni. Figures 9 and 15 only show a solubility around 12 at% Ni and 18 at% Ni, respectively, much lower than what is

expected from the binary phase diagram. Figure 39 from the current study shows a solubility at ~26 at%, consistent with the result of the binary phase diagram.

The  $\gamma$  corner of the  $\gamma + \beta + \alpha(\text{Mo})$  three-phase region is reported as Ni-13 at.% Al-41 at.% Cr in Figure 9 and Ni-12 at.% Al-44 at.% Cr in Figure 15. These data are in reasonable agreement. The composition of the same corner in Figure 39 is Ni-10.91 at.% Al-35.22 at.% Cr. The  $\gamma$  corner of the  $\gamma + \gamma' + \beta$  three-phase region in Figure 39 is at Ni-16.5 at.% Al-10.4 at.% Cr. In Figure 9 the corner is at Ni-15 at.% Al-18 at.% Cr. The increase in the solubility of Cr at a lower temperature does not conform to the pattern of behavior seen in the binary diagrams and calls into question the reliability of Figure 9. In all three diagrams the  $\gamma'$  phase appears to agree with one another.

The  $\beta$  phase region in Figures 39 and 40 differs greatly from that reported in Figures 9 and 15 where a maximum Cr solubility of 10 at.% is reported. The Cr solubility in  $\beta$  is reported to be essentially a constant value, independent of the Al concentration. In Figures 39 and 40, the  $\beta$  phase is observed to have a maximum solubility of Cr of 13.5 at.% and then decreases with increasing Al concentration to a minimum around 2.8 at.% Cr. There is some evidence to suggest that after this minimum there is a subsequent increase in the solubility of the Cr. More data can be collected from the diffusion multiple to define the shape of the  $\beta$  phase at higher Al concentration. Further work is recommended.

## **The Ni-Al-Mo Ternary System:**

The new Ni-Al-Mo ternary phase diagram in Figure 44 shows a phase previously unreported in the literature. This phase has a nominal composition of  $\text{Ni}_5\text{Al}_2\text{Mo}_8$ , and the narrow range of solubility that is observed in line scans 10, 12 and 13 of the Ni-Al-Mo diffusion multiple suggest that this phase is a stoichiometric compound. This phase can be seen in Figure 35, with line scans 10, 11, 12 and 13 crossing it. Line scan 11 is not reported in this study because the tie lines from this scan crossed the tie lines of the other three scans.

The  $\text{Ni}_5\text{Al}_2\text{Mo}_8$  phase is positioned in what has previously been reported as the  $\gamma' + \beta + \alpha(\text{Mo})$  three-phase region. That region as seen on the diagram in Figure 44 is divided into three two-phase regions and three-three phase regions. The two-phase regions are between the  $\gamma'$  and  $\text{Ni}_5\text{Al}_2\text{Mo}_8$  phases,  $\beta$  and  $\text{Ni}_5\text{Al}_2\text{Mo}_8$  phases and the  $\text{Ni}_5\text{Al}_2\text{Mo}_8$  and  $\alpha(\text{Mo})$  phases. The three-phase regions are among the  $\gamma' + \text{Ni}_5\text{Al}_2\text{Mo}_8 + \alpha(\text{Mo})$  phases, the  $\gamma' + \beta + \text{Ni}_5\text{Al}_2\text{Mo}_8$  phases, and the  $\beta + \text{Ni}_5\text{Al}_2\text{Mo}_8 + \alpha(\text{Mo})$  phases. There are two three-phase regions that appear in both Figure 44 and the previously reported phase diagrams, the  $\gamma + \delta + \alpha(\text{Mo})$  phases, and the  $\gamma + \gamma' + \alpha(\text{Mo})$  phases.

Both Figures 16 and 27 are at the same temperature (1200 °C) at which this study was undertaken. The  $\gamma$  phase region agrees in both Figures. In Figure 44, the  $\gamma$  phase agrees in general: there are two vertices where the two three-phase regions touch the single phase boundary. The two-phase regions that the  $\gamma$  phase borders on are also the same as those found in Figures 16 and 27. The shape of the two-phase regions is not the

same. The boundary between the  $\gamma$  and  $\gamma'$  phases is more curved in Figure 44. In Figure 44 the boundary has end points at the Ni-Al binary axis at Ni-20 at.% Al-0 at.% Mo, and at Ni-15.45 at.% Al-11.82 at.% Mo. The phase boundary moves rapidly to 20 at.% Al after leaving the binary axis. In Figures 16 and 27 the phase region intersects the Ni-Al binary axis at 18 at.% Al. Then the phase boundary move to points that are Ni-15 at.% Al-11 at.% Mo and Ni-15 at.% Al-15 at.% Mo. Figure 16 by Nash, Fielding and West shows good agreement with the  $\gamma$  corner of the  $\gamma + \gamma' + \alpha(\text{Mo})$  three-phase region in Fig. 44. The two-phase boundary between  $\gamma$  and  $\gamma'$  shows the same minimum of 16 at.% Al.

The  $\gamma$  corner of the  $\gamma + \delta + \alpha(\text{Mo})$  three-phase region in Figure 44 is at Ni-10.94 at.% Al-16.56 at.% Mo. In Figures 16 and 27, the same corner is at Ni-8 at.% Al-17 at.% Mo and Ni-7 at.% Al-17 at.% Mo. The Mo concentration of this corner agrees across the diagrams, however, the Al concentration does not. On the Ni-Mo binary axis the phase diagrams agree with one another and that there is a 26 at.% Mo solubility.

The  $\delta$  phase region agrees in all three diagrams. In Figure 44 this phase pushes 1 at.% Al further into the than the other two diagrams with the  $\delta$  corner of the three-phase region at Ni-1.7 at.% Al-19.9 at.% Mo.

The  $\gamma'$  phase region in Figure 44 also shows rough agreement with previous results with  $\gamma'$  corner of the  $\gamma + \gamma' + \alpha(\text{Mo})$  three-phase region at Ni-21.5 at.% Al-4.4 at.% Mo in Fig. 44 and Ni-23 at.% Al-6 at.% Mo in Figure 16 and Ni-21 at.% Al-5 at.% Mo in Figure 27. In all three diagrams the  $\beta$  and  $\alpha(\text{Mo})$  phases regions agree well.

# Conclusions

The discrepancies in the literature concerning the Ni-Al-Cr ternary phase diagrams have been partially addressed. The  $\alpha(\text{Cr})$  phase region has a different shape and solubility limits than those previously reported. The  $\beta$  phase also has a much different shape and solubility limits than previously reported results in the literature. The  $\gamma$  and  $\gamma'$  phases have much better agreement with the published data. The  $\gamma'$  phase boundaries agree with those in the literature whereas the  $\gamma$  phase boundaries do not agree with the published data.

In the Ni-Al-Mo system, a phase was observed with a composition of  $\text{Ni}_5\text{Al}_2\text{Mo}_8$  that has not been previously reported. This phase is believed to be a stoichiometric phase because of the narrow composition range observed. The data on the  $\beta$  phase that has been previously published is accurate, and the published data on the  $\gamma$ ,  $\gamma'$ , and  $\delta$  phases give the correct shape of the phase regions.

Further work in these systems is recommended to generate more tie-lines between the  $\alpha(\text{Cr})$  and  $\beta$  phases in the Ni-Al-Cr system to confirm the shape of both phases. More data can be collected from the same diffusion multiple to better define the composition regions of both the  $\gamma$  and  $\alpha(\text{Cr})$  phases. Isothermal sections at several temperatures will also need to be developed to provide accurate phase diagrams for the Ni-Al-Cr ternary

system. In the Ni-Al-Mo system, the two proposed three phase regions will need to be confirmed at 1200 °C. The structure and lattice parameters of the  $\text{Ni}_5\text{Al}_2\text{Mo}_8$  phase need to be determined to verify the existence of this phase, and the temperature stability of this phase needs to be investigated. Phase diagrams should also be generated at multiple temperatures to address the need for accurate phase diagrams for thermodynamic modeling.

One can see the amazing similarity between our measured Ni-Al-Cr isothermal section (Figure 39) and that calculated using the thermodynamic assessment of Huang and Chang<sup>4</sup> (Figure 46). The horseshoe shaped  $\alpha(\text{Cr})$  bcc phase region is very apparent in Figure 46. As a matter of fact, the thermodynamic assessment had a hard time reproducing the triangular (high solubility) shape of the  $\alpha(\text{Cr})$  phase region published before (Figures 8 and 9) without introducing very unrealistic parameters. It seems that the thermodynamic assessment has been right on this point. The observed  $\alpha(\text{Cr})$  phase region has a slightly higher solubility than the results of the calculation, indicating a slight adjustment of the thermodynamic parameter may be needed.

The shape of the  $\beta\text{-NiAl}$  phase region is another subject that deserves some discussion. The computed result (Figure 46) clearly shows a variable Cr solubility in  $\beta\text{-NiAl}$  with changing Al concentration, which agrees well with the experimental data of the current study (Figure 39). Previous studies (Figures 8 and 9) reporting almost a constant Cr solubility in  $\beta\text{-NiAl}$  seem doubtful, suggesting that the alloys used in those studies might not have reached equilibrium. The variable Cr solubility in  $\beta\text{-NiAl}$  is due to the variation of compositional point defect concentrations as Al composition is deviating

from the stoichiometric one.<sup>4</sup> Again, the thermodynamic assessment predicted this behavior against unreliable experimental results. This system is a good example showing the power of the CALPHAD approach in reconciling all the experimental data under a systematic thermodynamic framework to root out the reliable data.

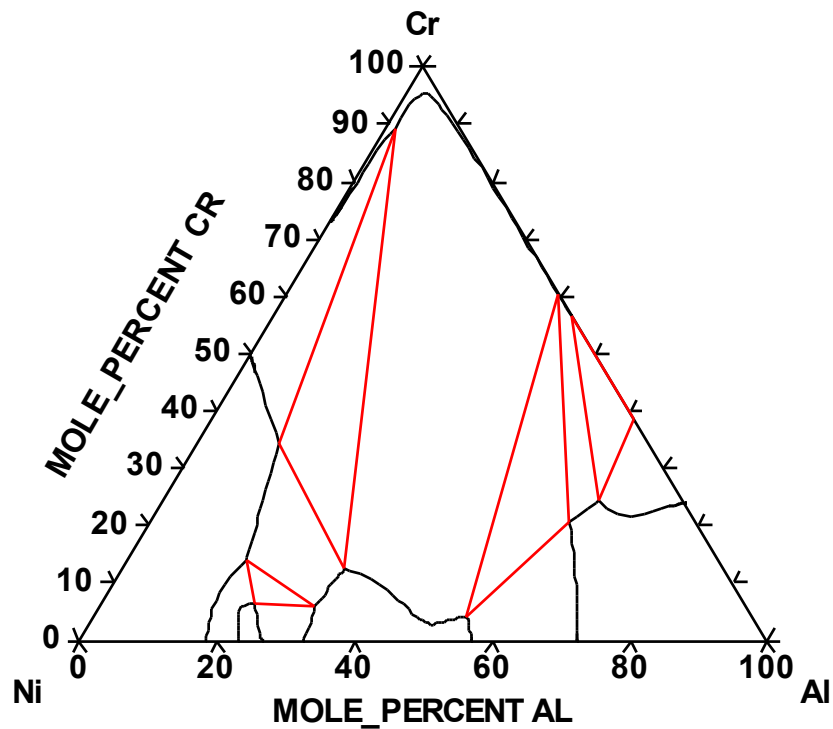


Figure 46. Calculated 1200 °C isothermal section of the Ni-Al-Cr ternary system based on the thermodynamic assessment of Huang and Chang.<sup>4</sup>

# References

- 
- <sup>1</sup> Fährmann M, Pollock TM, Johnson WC, Element partitioning during coarsening of ( $\gamma$ - $\gamma'$ ) Ni-Al-Mo alloys. *Metall. Mater. Trans. A.* (1997) **28A** 1943-1945.
- <sup>2</sup> Wu K, Zhou N, Pan X, Morral JE, Wang Y, Multiphase Ni-Cr-Al diffusion couples: A comparison of phase field simulations with experimental data. *Acta Mater.* (2008) **56** 3854-3861.
- <sup>3</sup> P. Nash, editor, Phase Diagrams of Binary Nickel Alloys, 1991 ASM International.
- <sup>4</sup> Huang W, Chang YA, Thermodynamic properties of the Ni-Al-Cr system. *Intermetallics* (1999) **7** 863-874.
- <sup>5</sup> Saunders N, The Al-Mo system (aluminum-molybdenum). *J. Phase Equili.* (1997) **18** 370-378.
- <sup>6</sup> Oforka NC, Argent BB, Thermodynamics of Ni-Cr-Al alloys. *J. Less-Common Met.* (1985) **114** 97-109.
- <sup>7</sup> Oforka NC, Haworth CW, Phase equilibria of aluminum-chromium-nickel system. *Scand. J. Metall.* (1987) **16** 184-188.
- <sup>8</sup> Hong YM, Mishima Y, Suzuki T, Accurate determination of  $\gamma'$  solvus in Ni-Al-X ternary systems. *MRS Symp. Proc.* (1988) **133** 429-440.
- <sup>9</sup> Brož P, Svoboda M, Buršik J, Kroupa A, Havránková J, Theoretical and experimental study of the influence of Cr on the  $\gamma + \gamma'$  phase field boundary in the Ni-Al-Cr system. *Mater. Sci. Eng. A* (2002) **325** 59-65.
- <sup>10</sup> Grushko B, Kowalski W, Pavlyuchov D, Przepiorzynski B, Surowiec M, A contribution to the Al-Ni-Cr phase diagram. *J. Alloys Comp.* (2008) **460** 299-304.
- <sup>11</sup> Nash P, Fielding S, West DRF, Phase equilibria in nickel rich Ni-Al-Mo and Ni-Al-W alloys. *Metal Sci.* (1983) **17** 192-194.

- 
- <sup>12</sup> Miracle DB, Lark KA, Srinivasan V, Lipsitt HA, Nickel-aluminum-molybdenum phase equilibria. *Metall. Trans. A* (1984) **15A** 481-486.
- <sup>13</sup> Maslenkov SB, Rodimkina VA, Phase equilibriums of the nickel-aluminum-molybdenum system in the region of nickel-nickel aluminide (NiAl)- molybdenum. *Metally* (1986) 218-223.
- <sup>14</sup> Maslenkov SB, Udovskii AL, Burova NN, Rodimkina VA, Phase diagram of the nickel-aluminum-molybdenum system at 1300-2000 C. *Metally* (1986) 198-205.
- <sup>15</sup> Maslenkov SB, Burova NN, Rodimkina VA, The nickel-nickel aluminide-molybdenum (Ni-NiAl-Mo) state diagram in the 1200-700 C temperature range. *Metally* (1988) 183-190.
- <sup>16</sup> Thompson RJ, Zhao J-C, Hemker KH, Effect of ternary elements on a martensitic transformation in  $\beta$ -NiAl. *Intermetallics* (2010) **18** 796-802.